https://doi.org/10.5194/egusphere-2026-2583
Preprint. Discussion started: 22 May 2026

Late Pleistocene temperature reconstruction of the interior Kalahari Plateau of Northwestern Botswana

Sameera Musa[1], Deepshikha Upadhyay[2], Alexandrea Arnold[2], Jamie Lucarelli[2], Bastien Linol[3], Daniel Gebregiorgis[4], Asfawossen Asrat[5,6], Aradhna Tripati[2,7]

[1]Department of Geoscience, Nelson Mandela University, Port Elizabeth, 6001, South Africa
[2]Department of Earth, Planetary and Space Sciences, Department of Atmospheric and Oceanic Sciences, Institute of the Environment and Sustainability, Center for Developing Leadership in Science, University of California, Los Angeles, USA
[3]AEON-ESSRI (Africa Earth Observatory Network-Earth Stewardship Science Research Institute), Nelson Mandela University, Port Elizabeth, South Africa
[4]Georgia State University, Atlanta, USA
[5]Department of Geology and Geological Engineering, School of Earth Sciences and Engineering, Botswana International University of Science and Technology
[6]School of Earth Sciences, Addis Ababa University, Addis Ababa, Ethiopia
[7]School of Earth Sciences, School of Geographical Sciences, University of Bristol, UK

Correspondence to: Sameera Musa (sam16musa@gmail.com)

Abstract

Late Quaternary climate reconstructions for southern Africa remain poorly constrained due to the scarcity of paleotemperature data, particularly across the interior, highly elevated Kalahari Plateau. This study addresses the gap by focusing on the Late Pleistocene period in Ngamiland of NW Botswana. We conducted an integrated and multi-proxy mineralogical and isotope geochemical study of marlstones, fossil gastropods, soil concretions, calcretes, and pan and lake sediments from short cores and outcrops of the Kalahari Group near the Tsodilo Hills. Our approach was applied to address the following objectives: (i) identify primary carbonates using petrographic screening, (ii) constrain the hydroclimate using $\delta^{13}C$ and $\delta^{18}O$ stable isotope signatures and processes, (iii) provide new age constraints of deposition using radiocarbon ^{14}C dating, and (iv) interpret paleotemperatures by analysing clumped isotopes (Δ_{47}) and dual clumped isotopes (Δ_{47}-Δ_{48}). This multi-proxy approach aimed at defining a robust proxy to reconstruct the Late Pleistocene climate in the interior Kalahari. Our studies revealed that the sediments were deposited between 49.05 ± 1.98 and 24.89 ± 0.13 ka BP ago based on ^{14}C calibrated ages (SHCal20). The marlstones, calcretes and soil concretions are micritic and sparitic with evidence of bioturbation, whereas fossil gastropods are devoid of reworking and suited for paleoclimate studies. The $\delta^{13}C$ and $\delta^{18}O$ values range between 0.1 and 4.2 ‰ VPDB and -0.3 and 9.4 ‰ VPDB, respectively while measured Δ_{47} temperatures range between -3.1 and 47.5 °C. Stable isotope variations suggest a strong biological control in the soil concretions, whereas the groundwater signature is likely overprinted in the calcretes, and a combination of meteoric and groundwater has influenced the texture of marlstones. The extreme temperatures are attributed to organic contaminants in the sediments. It is interpreted that fossil gastropods retain the primary geochemical

https://doi.org/10.5194/egusphere-2026-2583
Preprint. Discussion started: 22 May 2026

signatures based on the stable and clumped isotope variations and therefore represent the most reliable material for climate reconstructions in the region. Our study has provided the first direct temperature estimates of the Late Pleistocene for the interior Kalahari region from these gastropods which appear to be cooler than the present at ~15 °C. This study therefore addresses a major data gap in southern African paleoclimate records, which has implication for global climate models.

1 Introduction

Quaternary paleoclimate records in southern Africa are limited. Natural archives include speleothems (e.g. Shaw and Cooke, 1986; Chase et al., 2021), lake sediments (e.g. Ringrose et al., 2009; Burrough et al., 2009), and palynological assemblages (e.g. Cordova et al., 2017). Several proxies such as stable isotopes, pollen and diatom assemblages as well as organic biomarkers have been applied to interpret the paleoenvironment and paleoclimate in terms of fluctuating humid and arid episodes during the Pleistocene (Cordova et al., 2017; Kristen et al., 2007). However, developing a coherent model of the Quaternary paleoclimate of southern Africa remains challenging due to a paucity of terrestrial records across the region. Much of the existing understanding of Quaternary polar glaciations is derived from stable $\delta^{18}O$ and δD isotopes measured in ice core records from Antarctica (Vostok, Epica Dome C) and central Greenland (NGRIP and GISP2) (Jouzel et al., 2007; NGRIP Members, 2004), as well as from benthic foraminiferal $\delta^{18}O$ records from marine sediment cores (Shackleton et al., 1984; Zachos et al., 2008). Paleoclimatic reconstructions and models used to predict global warming are therefore geographically biased, especially in the Southern Hemisphere. This is of particular importance considering the far-reaching implications on global climate change policy and governance.

This study aims to narrow this gap by providing direct paleotemperature quantifications, which is a novel approach in the region. The late Quaternary Kalahari sediment cover in the region is a complex sedimentary setting due to periods of reworking, however, its widespread occurrence in the southern African region does provide opportunity to reconstruct the paleoclimate of the region with an integrated approach. Here, we present results from a multi-proxy investigation of a diverse set of carbonate archives, including calcrete, soil concretions, marlstones, gastropods, and lake sediments of the Kalahari sediments in Ngamiland, NW Botswana. Our approach utilises detailed petrography of the carbonates, radiocarbon ^{14}C age dating, stable carbon and oxygen isotope measurements, and carbonate clumped isotopes, which provide a direct constraint on mineral formation temperatures. To ensure the robustness of these estimates, carbonate preservation has been carefully evaluated to identify materials that yield reliable temperature estimates appropriate for climate and hydrological model simulations. This study thus provides the first direct temperature estimates for the interior Kalahari region thereby addressing a major data gap in southern African paleoclimate records, with important implications for global climate model inputs.

https://doi.org/10.5194/egusphere-2026-2583
Preprint. Discussion started: 22 May 2026

2 Background

2.1 Regional Climate

The Kalahari region is largely classified as a sub-humid to semi-arid climatic zone, with only its southwestern extent classified as arid (Figure 1). The position of the South African anticyclone and the Intertropical Convergence Zone (ITCZ) controls the rainfall variability with the regional climate system strongly influenced by moisture transport from both the Indian and Atlantic Oceans (Tyson and Preston-Whyte, 2000; Lutjeharms, 2006). Easterly circulation from the Indian Ocean provides the dominant source of summer rainfall, while the cold Benguela Current along the Atlantic margin suppresses convection and limits moisture availability in the western Kalahari, reinforcing a strong west–east rainfall gradient. Variability in rainfall on decadal timescales has been linked to large-scale climate oscillations such as El Niño, and may also reflect broader, hemispherical synchronous climate patterns (Nicholson, 2000). On longer, millennial timescales, orbital forcing is considered a key driver of shifts in the ITCZ, monsoon dynamics, and rainfall distribution across the southern African summer rainfall zone (Partridge et al., 1997; Marret et al., 2001).

The Ngamiland region of NW Botswana is in the semi-arid climatic zone of the central interior Kalahari Plateau. Mean annual temperatures range from ~18°C in the cooler months (June–August) to ~32°C in the austral summer (December–February), with average annual precipitation of 400–600 mm, mostly concentrated in the summer months (October–March). The Okavango River originates in the Angolan Highlands, where it is fed by austral summer rainfall before passing through the Caprivi Strip in Namibia and terminating in NW Botswana. Consequently, paleoclimate studies centred around the Okavango Delta are influenced by hydroclimatic factors further north.

https://doi.org/10.5194/egusphere-2026-2583
Preprint. Discussion started: 22 May 2026

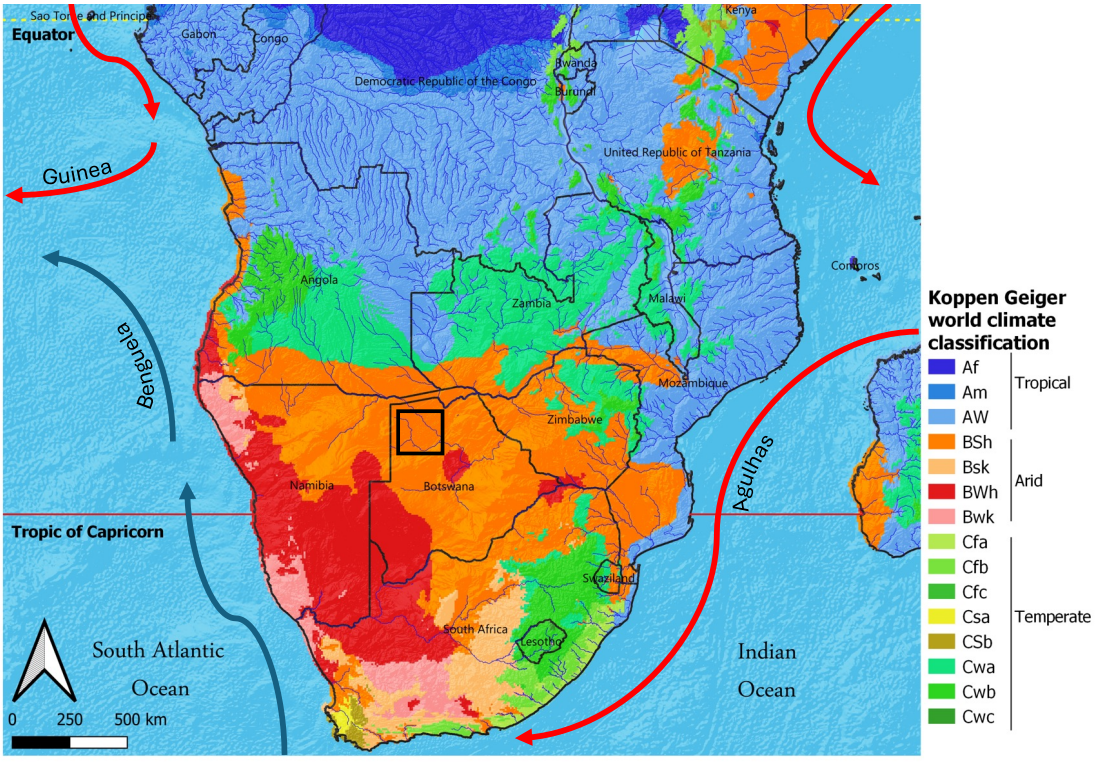

Figure 1: Climatic map of south-central Africa showing the studied location (black square) in the sub-humid to semi-arid zone.

Vast paleolakes, pans and rivers in the region are suggestive of previous wetter or more humid conditions. Located at the southwest end of the Okavango Delta, Lake Ngami is bounded to the south by the Kunyere Fault (Figure 2). Sedimentological and geochemical reconstructions of Lake Ngami sediments, based on ^{14}C and thermoluminescence dating techniques, estimate ages that range between 3.670 ± 0.030 ka and 40.499 ± 3.187 ka, between depths of 90 and 440 cm (Huntsman-Mapila, 2006; see also Shaw, 1985). The Makgadikgadi Pans to the southeast are older - dated between 41.24 ± 3.03 and 108.56 ± 9.02 ka using thermoluminescence dating techniques on siliceous sediments (Burrough et al., 2009). Further west, calcretes from the Etosha Pans in Namibia yield radiocarbon ages that range between 30 to 40 ka and younger organic residues that range between 3 and 19 ka (Brook et al., 2011). These records interpret multiple periods of arid and humid episodes in the Kalahari region; however, there is a lack of direct temperature quantification.

2.1 Regional Geology

The region is underlain by Precambrian granite and gneiss sequences of the Kalahari and Central African shields forming the bedrock, which includes the sporadic inselbergs of the Neoproterozoic Tsodilo Hills (Figure 2). The Cretaceous to Cenozoic-aged Kalahari Group unconformably overlie the basement sequences. Isolated paleolakes remain preserved among the outcropping basement inselbergs, such as the Paleolake Tsodilo (Figure 6; Geppert et al., 2021). The Kalahari Group comprises

https://doi.org/10.5194/egusphere-2026-2583
Preprint. Discussion started: 22 May 2026

a relatively thin veneer of duricrust and unconsolidated to semi-consolidated sediments (Linol, 2013; Musa, 2023) that currently stands at an elevation of about 1100 m a.s.l. (Doucouré and de Wit, 2003, Tinker et al., 2008). The unconformable contact between the basement and the Kalahari Group sediments marks a subcontinental peneplanation surface referred to as the African Erosion Surface. This surface is a significant episode in the regional geological evolution because it was formed as a result of the breakup of Gondwana and the beginning of the Kalahari Epeirogeny (King, 1963; de Wit, 2007; Linol et al., 2015). The epeirogeny was the key driver of exacerbated erosion and denudation that resulted in the deposition of the Kalahari Group.

Early works of Passarge (1904) identified four specific domains within the Kalahari Group. This includes the lowermost basal gravels and limestone of the Botletle Beds, unconformably overlain by various pan sequences of the Kalahari Kalk. Unconsolidated sediments of the Kalahari Sand overlie the Kalahari Kalk. The uppermost sequence comprises unconsolidated alluvium. The stratigraphy of the Kalahari Group is generally not well defined, and age constraints are limited. The sequences are constrained by a minimum Late Cretaceous age of 84 ± 4 Ma, based on a U-Pb perovskite of a kimberlitic intrusion within which xenoliths of the Kalahari Group are found (de Wit et al., 2017). In the more recent sediments, optically stimulated luminescence dating of linear sand dunes near Tsodilo Hills have been dated between 11.8 ± 1.6 and 98.1 ± 9.2 ka (Thomas et al., 2003). However, reworking of the dune fields in the northern Kalahari has provided inconsistent chronologies (e.g. Cooke, 1980; Thomas and Burrough, 2016). These uppermost unconsolidated sequences extend up to 2.5 million km^2.

The East African Rift System, which developed during the Oligo-Miocene, likely influenced the deposition of the upper sequences of the Kalahari Group sediments, as propagating rifts caused uplift, faulting, and subsequent graben formation of the basement rocks. This includes NE-SW oriented faults such as the Gumare and Kunyere faults. The underlying geology has thus had a significant influence on the drainage patterns in the Kalahari region. This is evident in the Kalahari Desert that paradoxically hosts the largest intra-continental alluvial fan — the Okavango Delta — which occurs in Ngamiland, Botswana (Figure 2). This sedimentary system is interpreted to be a graben structure of the East African Rift System across Precambrian basement (Modisi et al., 2000; Gumbricht et al., 2001) as evidenced from airborne magnetic surveys and sediment cores (Haddon, 2005).

Despite its significant geographical distribution, the Kalahari Group remains poorly constrained in age and depositional conditions. This is primarily attributed to the limited number of studies, paucity of outcrops showing the complete record, and scarcity of cores to the base of the Group. In addition, carbonates occurring within the Kalahari Group, which could be good indicators of paleoclimatic and paleoenvironmental setting during deposition, have been subject to intense physical weathering due to bioturbation and chemical weathering by surface and groundwater (Haddon and McCarthy, 2005; Linol et al., 2015).

https://doi.org/10.5194/egusphere-2026-2583
Preprint. Discussion started: 22 May 2026

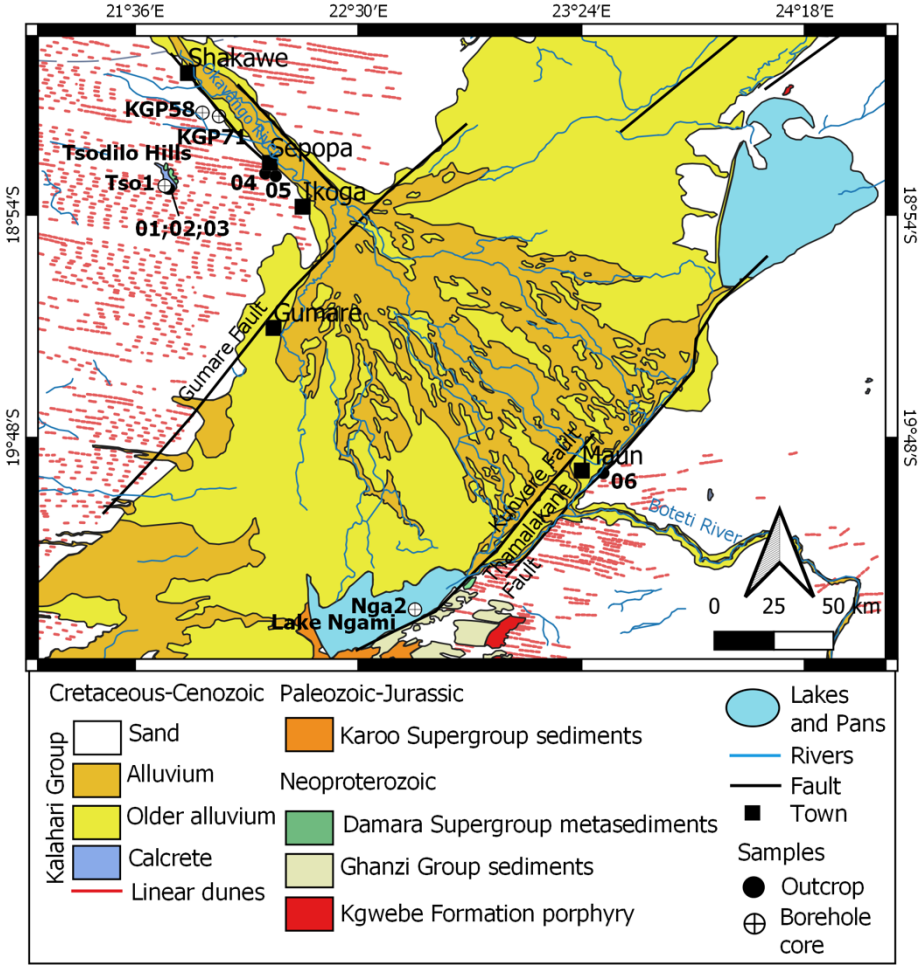

125 **Figure 2: Simplified geological map of the studied areas in Ngamiland, NW Botswana (after Mallick, 1978), with location of sampled outcrops and boreholes.**

3 Material and Methods

This study integrates field observations, petrography, and isotope geochemistry in order to understand the preservation state of the various carbonates, and to correctly interpret the proxy records.

130 3.1 Sampling

Selected samples from seven sites in the Kalahari region include marlstones, fossil gastropods, soil concretions, pan sediments, and modern shells (Table 1 and Appendix). The KGP borehole cores are housed at Tsodilo Resources Limited in Shakawe, Botswana. Two borehole cores, KGP 58 and KGP 71, drilled 7 km apart, west of the Okavango Panhandle are logged and sampled. Core Tso1 and Core Nga2, drilled close to the Tsodilo Hills and Lake Ngami, respectively, were studied by Linol

https://doi.org/10.5194/egusphere-2026-2583
Preprint. Discussion started: 22 May 2026

(2014). These are resampled for clumped isotope analysis. Outcropping sampling locations of Pleistocene age include Tsodilo Hills as well as a quarry in Sepopa, where marlstones, fossil gastropods, and soil concretions are sampled (Figure 2). Recent and modern carbonates are sampled to test the validity of clumped isotope thermometry and to identify which lake-to-air temperature transfer function best reproduces modern mean annual air temperature from different types of samples in the Kalahari region. Recent pan evaporites are sampled using an auger to the depth of 1.25 m; a surficial lake sample is collected from the margin of Barberspan; and a modern freshwater snail (*Canistes ovum sp.*) and a mussel (*Coelatura sp.*) from the Thamalakane River are analysed as analogues.

Table 1: Site location and elevations of carbonate samples collected

Locality	Site	Latitude	Longitude	Outcrop and borehole head elevation (m.a.s.l.)
Tsodilo Hills				
	Core Tso1	-18.78277778	21.71972222	1007
	Outcrop 01	-18.79406300	21.73804900	1000
	Outcrop 02	-18.79303900	21.73041000	1008
	Outcrop 03	-18.79408900	21.73637400	1003
Shakawe				
	Core KGP58	-18.4877590	21.87189000	1013
	Core KGP71	-18.50188100	21.93858900	992.5
Sepopa				
	Outcrop 04	-18.73280753	22.12561667	994
	Outcrop 05	-18.74356858	22.16715800	989
Lake Ngami				
	Core Nga2	-20.49416667	22.72888889	925
Maun				
	Outcrop 06	-19.94329100	23.48853400	944
Kang				
	Core Ka	-23.69899600	22.80246800	1122
Barberspan				
	Outcrop 07	-26.58985800	25.60346700	1331

https://doi.org/10.5194/egusphere-2026-2583
Preprint. Discussion started: 22 May 2026

3.2 Petrographic screening

Petrographic screening using a light microscope was conducted at Nelson Mandela University to identify the different carbonate microfabrics, such as micritic and sparitic phases, in order to assess the preservation states of the various samples.

3.3 Radiocarbon dating

Radiocarbon dating was conducted on 11 marlstones and fossil gastropod samples of the *Bulinus* and *Radix* species at the UCI Keck-CCAMS facility (Table 5). The samples were leached with 10 % HCl prior to analysis with 85 % phosphoric acid. All results are corrected for isotopic fractionation according to the conventions of Stuiver and Polach (1977), with $\delta^{13}C$ values measured on prepared graphite using the AMS spectrometer. Radiocarbon concentrations are given as fractions of the modern standard, D14C, and conventional radiocarbon age, following the conventions of Stuiver and Polach (1977).

3.4 $\delta^{13}C$ and $\delta^{18}O$ isotope analysis

Stable carbon and oxygen isotopes were measured on 18 carbonate samples at the University of Cape Town (Table 3). Samples were powdered either by drilling using a Dremel at low speed with dental drill bits attached or homogenization using a mortar and pestle. Between 0.25 and 0.4 mg of the collected carbonate powder was weighed into 12 ml borosilicate tubes kept at a temperature of 72 °C. The tubes were flushed with helium to remove atmospheric air using the CTC Analytics A200S autosampler. Each sample was digested with 5 to 7 drops of a mixture of 85 % Orthophosphoric acid and Phosphorus pentoxide (SG of solution = 1.92). The acid digestion reaction was 2.5 h. The evolved gas was drawn through a Thermo Finnigan model II gasbench, where it passed through a Nafion water removal unit. Following this, the Poraplot Q GC column separated the gas compounds released by the reaction before the gas was drawn through a second Nafion water trap. The purified gas was released into the gas bench to a Delta Plus XP isotope ratio mass spectrometer (Thermo Electron, Bremen, Germany). The unit was controlled by Isodat software that recorded the $\delta^{13}C$ and $\delta^{18}O$ values. The gas flow was controlled to give 8 sample peaks and 5 reference peaks to which the gas was standardized. The CO_2 reference gas of 99.995 % purity was introduced into the mass spectrometer via the gas bench and controlled by the Isodat software. The Cavendish Marble in-house standard and the international Carrara Z & IAEA-CO8 standards were used.

3.5 Carbonate clumped isotope thermometry

Given the lack of direct temperature estimates for the late Quaternary of the interior of southern Africa, the novel technique of clumped isotope thermometry provides a significant tool for climate reconstructions. The technique is based on the thermodynamic preference of the rare isotopes of carbon and oxygen, ^{13}C and ^{18}O, to bond or clump together to form clumped isotopes. These isotopologues are distinguishable based on the differences in zero-point energies and record fractionation processes similar to conventional stable isotopes, while being independent of the isotopic composition (Ghosh et al., 2006; Eiler, 2007).

https://doi.org/10.5194/egusphere-2026-2583
Preprint. Discussion started: 22 May 2026

The most frequently reported clumped isotopologues is mass- 47 CO_2 (^{18}O-^{13}C-^{16}O). The abundance of this isotopologue beyond what would be expected based on statistics alone is expressed as:

$$\Delta_{47} = \left[\frac{R^{47}}{R^{*47} - 1} - \frac{R^{46}}{R^{*46} - 1} - \frac{R^{45}}{R^{*45} - 1}\right] - 1$$

Where R^{47}, R^{46}, and R^{45} are the measured ratio of isotopologues 47/44, 46/44, and 45/44, respectively. R* represents the isotopologues in a stochastic distribution, calculated based on reference gases that have been heated to 1000 °C (Affek and Eiler, 2006). The resultant Δ_{47} value is used to determine the temperature of carbonate precipitation or recrystallization. This calculated temperature is used to back-calculate the $\delta^{18}O$ value of the source water from which the carbonate precipitated.

More recently, higher precision in mass spectrometry has allowed for the simultaneous measurement of both Δ_{47} and Δ_{48}. The latter refers to the measurement of the multiply substituted isotopologue ^{18}O-^{12}C-^{18}O. This paired analysis, termed dual clumped isotopes, may be used to identify or interpret kinetic effects in carbonates in addition to calculating the temperature (Fiebig et al., 2019; Bajnai et al., 2020).

The primary advantage of clumped isotope thermometry is the homogeneous equilibrium of the obtained temperature, i.e., the constituents are in a single phase independent of the bulk isotopic composition. This eliminates the complexity of added phases that the carbonate mineral may have formed in, effectively addressing the major drawback of the inferred $\delta^{18}O$ value of the ambient water when applying the carbonate-water isotopic temperature scale (Urey, 1947). A direct estimation of the temperature at which the carbonate formed is thus possible.

3.5.1 Sample preparation

A total of 23 carbonate powders were prepared and analysed at the Eagle-Tripati laboratory at UCLA (Table 4 and Table 5). Biogenic carbonates were cleaned by sonication at 5-minute intervals so as not to introduce heat and were further cleaned with sharp tools under a microscope before being homogenised with a mortar and pestle. Calcrete and marlstone samples were drilled using a Dremel at low speed with dental drill bits attached. The carbonate content was calculated by loss on ignition (Heiri et al., 2001). Sample replicates analysed on the Thermo Fisher MAT 253 had masses between 6–11 mg, and sample replicates analysed on the Nu Perspective instruments had masses between 0.35–0.49 mg. The powder was weighed into silver capsules prior to analysis.

3.5.2 Instrumentation

Three mass spectrometers were used to measure Δ_{47} and Δ_{48}. A Thermo Fisher MAT 253 gas source dual inlet mass spectrometer was used to measure Δ_{47}, and two Nu Instruments Perspective gas source dual inlet mass spectrometers were used to simultaneously measure Δ_{47} and Δ_{48}. A detailed description of the methods used here, along with inter-instrument data comparisons and statistical analyses have been reported previously (Defliese and Tripati, 2020; Upadhyay et al., 2021; Lucarelli et al., 2023a; Lucarelli et al., 2025).

https://doi.org/10.5194/egusphere-2026-2583
Preprint. Discussion started: 22 May 2026

For each instrument, an analytical session consists of an equal number of standards and samples, where standards bracket the samples at the beginning and end of the session. Acid digestion of the sample powders was performed at 90 °C in a common acid bath to produce the resultant CO_2 gas, which was then cryogenically purified in a purification autoline modelled after Passey et al. (2010) to remove water and other contaminants. The purified gas was then transferred into the respective instruments. A minimum of 3 replicates per sample were analysed to reduce the uncertainty.

For each replicate, the MAT 253 spectrometer acquires 9 blocks of data, where each block contains 10 cycles. Each cycle consists of 8 s of integration and 16 s of changeover delay, yielding a total integration time of 720 s per replicate. Replicate measurements on the Nu Perspectives were conducted in three acquisition blocks of 20 cycles each. Each cycle included 20 s of integration followed by an 8 s changeover delay, resulting in a total integration time of 1,200 s. For all instruments, *m/z* 44, 45, and 46 are registered through 3×10^8, 3×10^{10}, and 10^{11} Ω resistors, respectively. The detectors for *m/z* 47–49 are registered through 10^{12} Ω resistors. Isotopic values are measured relative to an Oztech reference gas with the values $\delta^{18}O$= 25.03 ‰ VSMOW and $\delta^{13}C$= 3.60 ‰ VPDB. The reference gas is maintained at a room temperature of ~ 22 °C.

3.5.3 Data Processing and Corrections

Data were processed using Easotope software (John and Bowen, 2016), and by applying the correction parameters of Brand et al. (2010). These are based on $\delta^{13}C$ measurements determined on CO_2 and corrected for the amount of ^{17}O. The carbonate standards used in empirical transfer functions (Dennis et al., 2011) include ETH-1, ETH-2, and ETH-3 (Bernasconi et al., 2018; 2021), with in-house standards Carrara Marble Tile, and Veinstrom (Lucarelli et al., 2023a; 2023b; 2025). Carbonate standards ETH-1 and ETH-2 were used on the Nu Perspectives for linearity corrections, while the MAT 253 used ETH-1, ETH-2, and gas standards equilibrated at 25 and 1000 °C. The gas standards have bulk isotope values with a difference of ~60 ‰ in their δ_{47} value. Bonedry DI is a gas from an Airgas CO_2 cylinder and represents the lower endmember, whereas Evap DI + CM is a standard prepared in-house from digesting Carrara Marble.

Final corrected sample values were reported on the Intercarb-Carbon Dioxide Equilibrium Scale (I-CDES; Bernasconi et al., 2021). The measured Δ_{47} values were interpreted as temperatures using the calibration of Anderson et al. (2021), given the wide range of temperatures this is applicable to. The measured Δ_{48} values were interpreted as temperatures using the calibration of Fiebig et al. (2021), given the wide range of temperatures this is applicable to.

3.6 Temperature reconstruction

A transfer function was applied to correlate the Δ_{47} values of the lake sediments and shells to mean annual air temperatures (MAAT).

The transfer function of Hren and Sheldon (2012) was calculated from 88 lake sediments, with most occurring in the northern hemisphere. This highlights the need to test the validity of the transfer function in the Kalahari, in the Southern Hemisphere. Modern samples were used to test the validity of clumped isotope thermometry as well as the applied transfer function on different types of samples in the studied area. More recently, the applied transfer functions of Terrarez et al. (2025) are based

https://doi.org/10.5194/egusphere-2026-2583
Preprint. Discussion started: 22 May 2026

on a much larger dataset. In this study, we compare the calculated MAAT from both studies to the modern analogues in order to determine which function is best suited.

4. Results

4.1 Lithostratigraphy of the Kalahari Group

Two drill cores, KGP 58 and KGP 71, intersect a basement of weathered gneiss at depths of 47 and 68 m, respectively (Figure 3). These sections show basal conglomerates and fine to coarse-grained sandstones grading upward into fine to coarse-grained variegated sands. The upper, poorly consolidated sequence comprises marlstones (Figure 4) and carbonate sands with chalky textured concretions interpreted to represent Bk soil horizons. In the Tso1 drill core, the equivalent Kalahari Group section is 42 m thick, overlying a silcrete (Linol et al., 2013). It comprises 30 m of unconsolidated aeolian sand overlain by fossiliferous grey marlstones and soil concretions. In contrast, the 125 m deep drill core at Lake Ngami (site Nga-2), comprises almost exclusively fine sands with organic-rich muddy horizons as interpreted from the drill cuttings. Sample descriptions are summarized in the appendix.

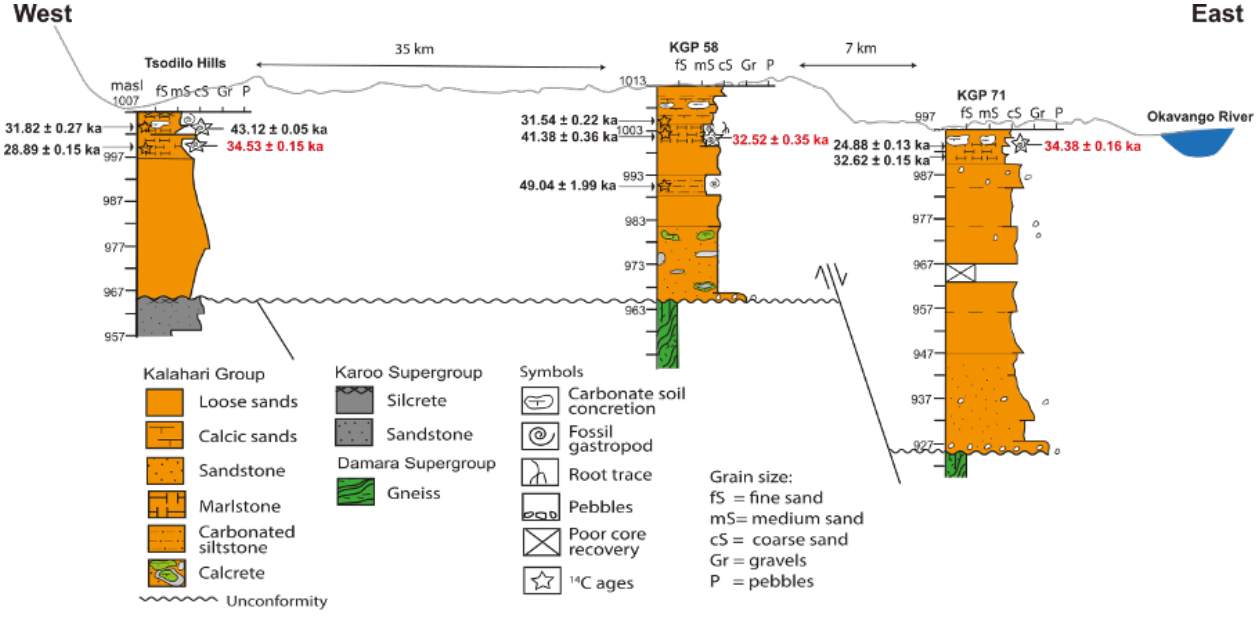

Figure 3: Sedimentological logs of Tso1 (Tsodilo Hills), KGP58, and KGP71 drill cores (Figure 1 for location). At KGP58, radiocarbon dates of a fossil gastropod and sediments between 8 and 23 m range between 49 and 31 ka BP (see Table 2), which reveal a sedimentation rate of ca. 0.8 m per thousand years.

4.2 Radiocarbon ages

The measured ^{14}C calibrated ages (SHCal20) of the Kalahari Group marlstones and fossil gastropods range between 49.0 ± 1.9 ka and 24.8 ± 0.1 ka (Table 1). These data are calibrated according to SHCal20. The oldest date is from a depth of 23 m in

https://doi.org/10.5194/egusphere-2026-2583
Preprint. Discussion started: 22 May 2026

borehole core KGP 58, whereas the youngest date is from a depth of 4.5 m in borehole core KGP 71 (Figure 3). Fossil gastropods yield ^{14}C results with a smaller range in comparison to the marlstones. Radiocarbon dating results on modern gastropods from the region indicate present-day ages (Riedel et al., 2014), therefore, the fossil gastropods in this study are not corrected for any reservoir effect, as it has been shown that old carbon is not readily incorporated into shells.

Table 2: Radiocarbon ages of selected carbonates from Ngamiland, Botswana (see Figure 2 for location and appendix for sample description).

Sample name	^{14}C age ka	SHCal20 ka	Elevation (m a.s.l.)
01_a	24670 ± 150	28.89 ± 0.15	1000
01sn_a	30160 ± 190	34.53 ± 0.15	1000
03_b	27930 ± 220	31.82 ± 0.27	1003
03sn_e	39810 ±600	43.12 ± 54.5	1003
KGP58_e	27660 ±240	31.54 ± 0.22	1005
KGP58_f	36430 ± 480	41.38 ± 0.36	1002
KGP58sn_a	28420 ± 160	32.52 ± 0.35	1002
KGP58_h	46400 ± 1600	49.05 ± 1.98	990
KGP71_b	20680 ± 70	24.89 ± 0.13	992.5
KGP71_e	28520 ± 170	32.62 ± 0.15	991.5
KGP71sn_a	29930 ± 220	34.38 ± 0.16	991.5

4.2 Petrographic screening

The calcitic microfabrics of the marlstones in the core and the outcrops are both micritic and sparitic (Figure 4 and Figure 5). However, the primary matrix is micritic. Evidence of root traces and bioturbation is preserved, which are indicative of pedogenic processes. Preserved shell fragments and quartz grains exhibit dissolved boundaries indicative of alkaline conditions (Figure 5). Outcropping marlstones also preserve reprecipitated needle-fibre textured calcic microfabrics. In places, the marlstones are diatomaceous within a micritic fabric that is capped by a thin layer of calcrete (e.g. Figure 6 i).

https://doi.org/10.5194/egusphere-2026-2583
Preprint. Discussion started: 22 May 2026

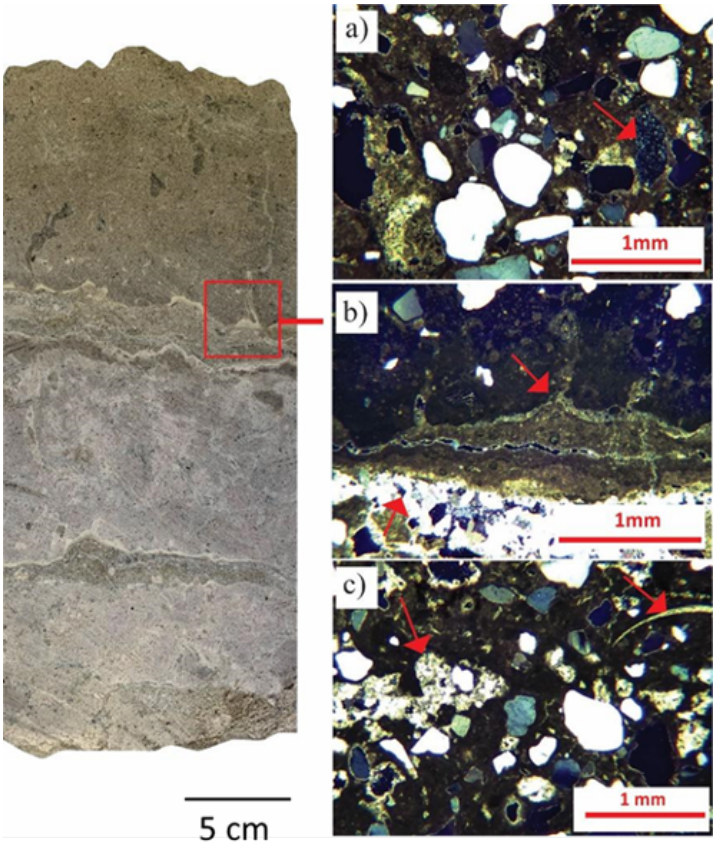

Figure 4: KGP 58 core (see Figure 3 for location) and thin sections from a sample at a depth of 8.3 m from this core. The grey-green biomicritic groundmass in the upper 15 cm preserves root traces indicating pedogenic processes. In the photomicrographs, which is of the red square on the core section: a) quartz grains are poorly sorted with dissolved boundaries, indicating alkaline conditions, within a predominantly micritic matrix (arrow); b) a laminar micritic layer (upper arrow) directly overlies a sandy matrix (lower arrow); and c) bioturbation structure is filled with sparite (indicated with arrow on the right) and visible shell fragments (indicated with arrow on the right).

https://doi.org/10.5194/egusphere-2026-2583
Preprint. Discussion started: 22 May 2026

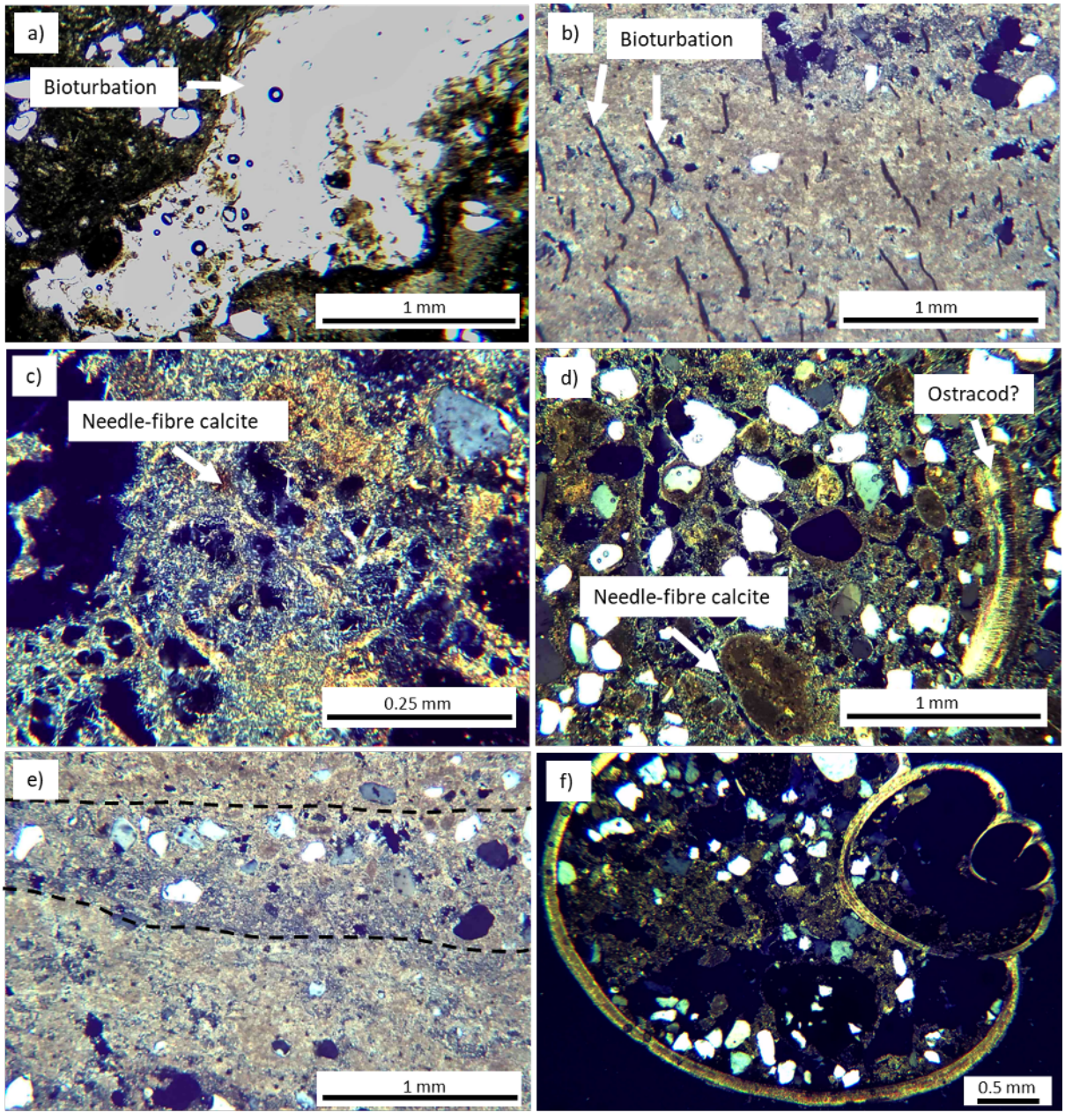

Figure 5: Microphotographs of selected samples from Tsodilo Hills (see Figure 2 for location). a) Bioturbation in a micritic marlstone (sample 01_b); b) Bioturbation in micritic marlstone with laminar structures (sample 02_c); c) Needle-fibre calcite indicative of reprecipitation within a white chalky groundmass (sample 03_a); d) Needle-fibre calcite and micritic matrix with coarse sub-rounded quartz grains surrounded by microsparitic halos indicative of reprecipitation; fragments of ostracods are visible (sample 03_b) e) laminar calcrete with sandy layers (sample 02_d); and f) freshwater fossil mollusc (*Bulinus sp.*) filled with a sandy and calcitic matrix (sample 03sn_b).

https://doi.org/10.5194/egusphere-2026-2583
Preprint. Discussion started: 22 May 2026

4.3 Stable carbon and oxygen isotopes and carbonate clumped isotopes

Stable isotope values vary by carbonate type and texture (Figure 7). Results are presented in Tables 2, 3, and 4. Measured $\delta^{13}C$ and $\delta^{18}O$ values of the fossil gastropods range between -2.3 and -0.3 ‰ VPDB and -6.3 and 2.3 ‰ VPDB, respectively. In marlstones, $\delta^{13}C$ and $\delta^{18}O$ values range between -5.8 and 1.9 ‰ VPDB and -9.6 and -1.02 ‰ VPDB respectively. Calcretes yield $\delta^{13}C$ values with a relatively small range between -0.23 and -1.05, and $\delta^{18}O$ values with a relatively large range between -8.46 and -3.57 ‰ VPDB. In contrast measured $\delta^{13}C$ values in Bk horizons range between –5.10 and 1.0 ‰ VPDB and $\delta^{18}O$ values range between –8.5 and –7.8 ‰ VPDB. Marls yield $\delta^{13}C$ values that range between -1.56 and 5.01 ‰ VPDB and $\delta^{18}O$ values that -0.90 and 0.26 ‰ VPDB. Near surface pan evaporites yield $\delta^{13}C$ values that range between 0.05 and 4.22 ‰ VPDB and significantly higher $\delta^{18}O$ values in comparison to other samples, ranging between 0.65 and 9.44 ‰ VPDB.

The Δ_{47}-derived temperatures of the carbonates (Table 4 and Table 5) range between –3.1 ± 3.6 ºC and 47.5 ± 5.8 ºC. The lowest reconstructed temperature (−3.1 ± 3.6 °C) was obtained from drill cuttings at Lake Ngami at a depth of 44 m. This anomalously low value likely reflects contamination. The highest temperature of 47.5 ± 5.8 ºC is measured from Kang Pan evaporites. In fossil gastropods, the derived Δ_{47} temperatures range between 13.8 ± 2.2 and 19.9 ± 1.5 ºC. In marlstones and calcretes, there is a large variation in the derived Δ_{47} temperatures between 11.2 ± 5.3 ºC and 24.3 ± 4.5 ºC.

https://doi.org/10.5194/egusphere-2026-2583
Preprint. Discussion started: 22 May 2026

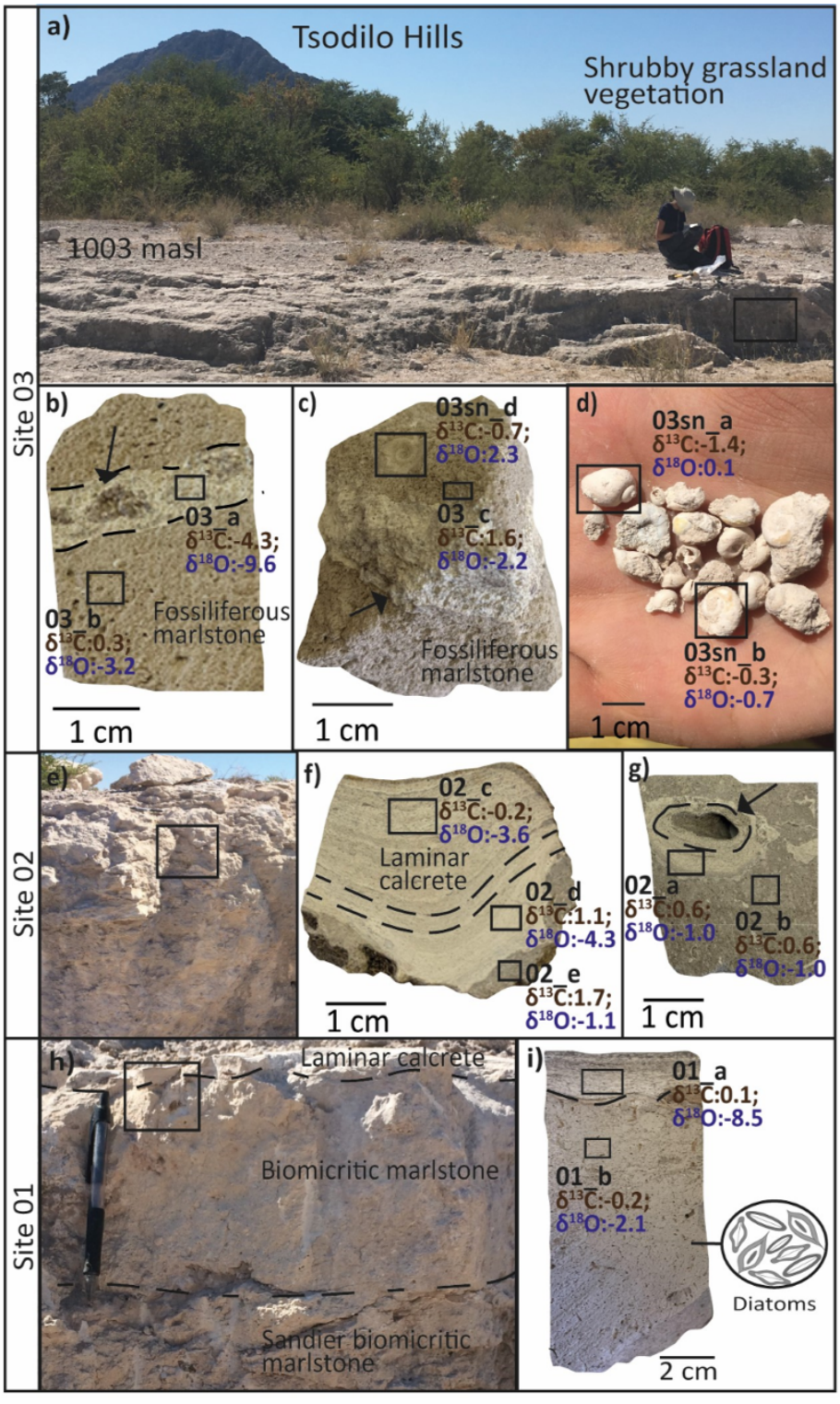

https://doi.org/10.5194/egusphere-2026-2583
Preprint. Discussion started: 22 May 2026

Figure 6: Sampled outcrops at Tsodilo Hills (see Figure 2 for location): a) Site 03, where 6 samples were analysed for isotope analyses; b) chalky textured carbonate vein intersecting fossiliferous marlstone; c) a fossil gastropod of the *Bulinus sp*. and marlstone matrix; d) *Radix sp.* and *Bulinus sp.* fossil gastropods; e) Quarry face of site 02, where 5 samples were collected and analysed for isotope analyses; f) laminar calcrete and fossiliferous marlstone; g) rhyzolith carbonate precipitates around a tubular cavity and fossiliferous marlstone; h) Quarry face of site 01, where 2 samples were collected and analysed for isotope analyses; and i) laminar calcrete and marlstones with diatom fossils, which indicate a fluvial-lacustrine depositional environment.

https://doi.org/10.5194/egusphere-2026-2583
Preprint. Discussion started: 22 May 2026

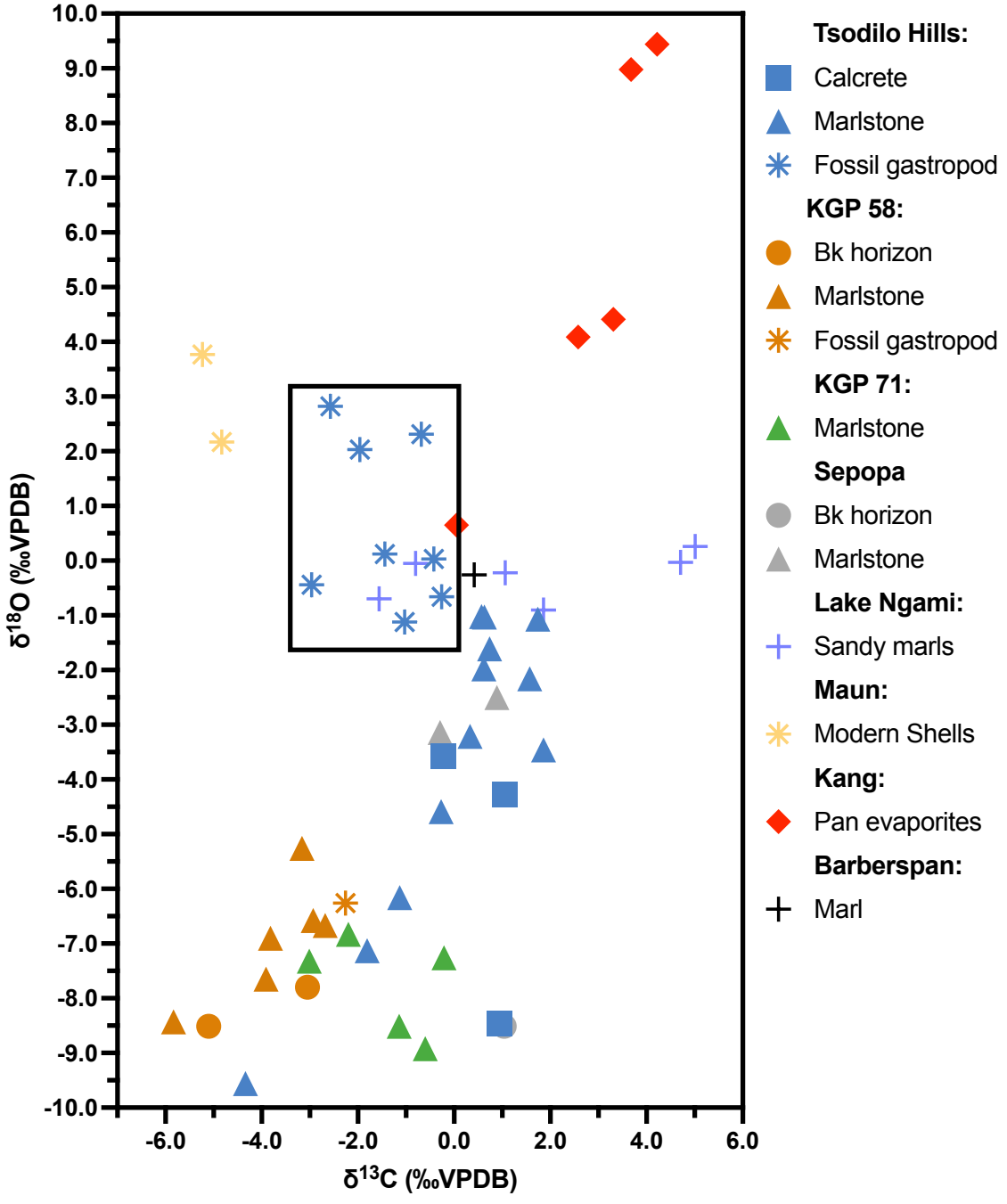

Figure 7: $\delta^{13}C$ versus $\delta^{18}O$ values of measured Kalahari Group sediments, soil concretions, and fossil gastropods. The evaporites (diamonds) have significantly higher $\delta^{18}O$ values compared to the other samples due to the influence of evaporation. $\delta^{18}O$ values in fossil and modern shells (black square delineates fossil gastropods) are distinctively higher compared to the marlstone (triangles), and close to 0.

https://doi.org/10.5194/egusphere-2026-2583
Preprint. Discussion started: 22 May 2026

Table 3: Stable carbon and oxygen isotope analyses on selected marlstones, fossil gastropods, and pan sediments.

Sample name	$\delta^{13}C$ (‰ VPDB)	1s.d	$\delta^{18}O$ (‰ VPDB)	1s.d	$\delta^{18}O$ (‰ VSMOW)	1s.d
Tso1_c	-1.13	0.11	-6.16	0.12	-6.16	0.12
02_c	-0.23	0.05	-3.57	0.09	-3.57	0.09
02_d	1.05	0.03	-4.27	0.09	-4.27	0.09
02_e	1.74	0.17	-1.07	0.16	-1.07	0.16
03_c	1.57	0.12	-2.16	0.11	-2.16	0.11
03sn_d	-0.68	0.15	2.31	0.18	2.31	0.18
KGP58_a	-3.05	0.16	-7.80	0.11	-7.80	0.11
KGP58_b	-5.10	0.18	-8.51	0.12	-8.51	0.12
KGP58_c	-3.16	0.07	-5.26	0.09	-5.26	0.09
KGP58_d	-2.93	0.21	-6.58	0.24	-6.58	0.24
KGP58_g	-2.68	0.06	-6.67	0.07	-6.67	0.07
KGP58sn_b	-2.26	0.12	-6.26	0.14	-6.26	0.14
KGP71_a	-0.60	0.05	-8.92	0.11	-8.92	0.11
KGP71_c	-2.20	0.08	-6.83	0.12	-6.83	0.12
KGP71_d	-0.21	0.14	-7.26	0.19	-7.26	0.19
04_b	0.89	0.17	-2.50	0.21	-2.50	0.21
Ka_e	4.22	0.24	9.44	0.20	9.44	0.20
Ka_c	3.31	0.23	4.41	0.18	4.41	0.18

Table 4: Carbonate clumped isotope analyses on selected marlstones, fossil gastropods, pan and lake sediments.

Sample name	Replicates	$\delta^{13}C$ (‰VPDB)	1 s.d	$\delta^{18}O$ (‰VPDB)	1 s.d	Δ_{47} avg	1 s.e	Δ_{47} T (°C)	1 s.e	$\delta^{18}Ow$ (‰VSMOW)	1 s.d
Tso1_a	4	-0.3	0.1	-4.6	0.1	0.699	0.006	19.3	1.8	-3.4	0.8
Tso1_b	2	-1.8	0.1	-7.1	0.1	0.726	0.018	11.2	5.3	-7.7	1.8
Tso1_d	4	1.9	0.0	-3.5	0.0	0.711	0.010	15.7	3.0	-3.0	1.4
01_a	2	1.0	0.0	-8.5	0.1	0.612	0.029	19.6	9.1	-7.2	1.9
01_b	5	0.7	0.1	-1.6	0.1	0.607	0.011	20.8	4.8	-6.0	1.5
01_c	2	0.6	0.1	-2.0	0.0	0.615	0.012	18.2	3.8	-1.0	0.8
02_a	5	0.6	0.1	-1.0	0.3	0.633	0.011	12.8	3.3	-1.2	0.8
02_b	5	0.6	0.0	-1.0	0.1	0.617	0.004	17.4	1.3	-0.2	0.3
03_a	4	-4.3	0.1	-9.6	0.1	0.608	0.009	20.5	3.1	-8.1	0.6
03_b	4	0.3	0.1	-3.2	0.2	0.597	0.014	24.3	4.5	-1.0	1.0
03sn_a	4	-1.4	0.1	0.1	0.4	0.628	0.010	14.3	3.0	0.2	0.7
03sn_b	4	-0.3	1.2	-0.7	1.5	0.613	0.005	18.9	1.4	0.5	0.9
03sn_c	4	-1.0	0.1	-1.1	0.1	0.629	0.007	13.8	2.2	-1.1	0.5
KGP58_e	2	-3.8	0.1	-6.9	0.2	0.601	0.006	22.8	1.8	-5.0	0.2
KGP58_f	3	-3.9	0.0	-7.7	0.1	0.616	0.005	17.7	1.5	-6.8	0.3
KGP58_h	2	-5.8	0.2	-8.4	0.5	0.632	0.012	12.9	3.6	-8.6	0.4
KGP71_b	3	-1.1	0.1	-8.5	0.1	0.611	0.005	19.5	1.5	-7.3	0.3
KGP71_e	5	-3.0	0.0	-7.3	0.0	0.616	0.018	18.5	5.6	-6.4	1.2
04_a	3	-0.3	0.0	-3.1	0.1	0.694	0.003	21.1	1.0	-1.5	0.5
05_c	3	1.0	0.0	-8.5	0.0	0.673	0.012	25.0	3.4	-6.2	1.2
Nga2_a	3	-0.8	0.0	-0.1	0.0	0.751	0.014	4.2	3.9	-2.2	1.6
Nga2_b	2	-1.6	0.1	-0.7	0.2	0.669	0.065	32.1	23.4	2.8	6.6
Nga2_c	3	1.1	0.6	-0.2	0.2	0.779	0.014	-3.1	3.6	-4.1	1.7
Nga2_d	2	1.9	0.2	-0.9	0.2	0.673	0.035	28.8	12.3	2.2	3.2
Nga2_e	3	5.0	0.0	0.3	0.1	0.763	0.006	0.9	1.6	-2.7	0.7

Nga2_f	2	4.7	0.2	0.0	0.3	0.664	0.075	34.9	27.6	3.9	7.2
06_a	3	-4.8	0.2	2.2	0.1	0.595	0.001	24.7	0.5	4.5	0.1
06_b	4	-5.2	0.2	3.8	0.2	0.599	0.008	23.3	2.6	5.8	0.5
Ka_a	3	0.1	0.2	0.7	0.2	0.645	0.005	9.2	1.4	-0.3	0.4
Ka_b	4	2.6	0.1	4.1	0.2	0.605	0.007	21.3	2.3	5.7	0.4
Ka_d	3	3.7	0.0	9.0	0.2	0.535	0.014	47.5	5.8	15.7	0.9
07_a	4	0.4	0.1	-0.3	0.2	0.631	0.010	13.2	3.1	-0.4	0.7

Table 5: Dual clumped isotope analysis of fossil gastropods

Sample name	**Replicates**	**$\delta^{13}C$ (‰VPDB)**	**1 s.d.**	**$\delta^{18}O$ (‰VPDB)**	**1 s.d.**	**Δ_{47} avg**	**1 s.e.**	**Δ_{48} avg**	**1 s.e.**	**Δ_{47} T (°C)**	**1 s.e.**	**Δ_{48} T (°C)**	**1 s.e**	**$\delta^{18}Ow$ (‰VSMOW)**	**1 s.d.**
03sn_e	6	-2.6	0.3	2.8	0.4	0.609	0.00	0.274	0.02	19.9	1.5	14.3	4.8	4.2	0.5
03sn_f	7	-2.0	0.2	2.0	0.4	0.614	0.01	0.255	0.03	18.4	1.8	23.6	9.3	3.1	0.3
03sn_g	6	-3.0	0.2	-0.4	0.4	0.613	0.01	0.266	0.01	18.7	2.1	18.7	2.7	0.7	0.3

https://doi.org/10.5194/egusphere-2026-2583
Preprint. Discussion started: 22 May 2026

4.4 Validity of the clumped isotope geothermometer

Recent and modern samples analysed to test the validity of clumped isotope thermometry include freshwater shells, as well as pan and lake sediments. The $\delta^{13}C$ and $\delta^{18}O$ measurements reveal similar values with an average of -5 and 3‰ VPDB, respectively, regardless of whether it was the *Canistes ovum sp.* or *Coelatura sp.* The modern biogenic carbonates reveal a combined average temperature of 24.0 ± 1.1 °C (Table 4), which is in agreement with modern water temperatures (values of 23.9 °C +/- 4.2 °C; Oromeng et al., 2021). These findings demonstrate that the geothermometer is valid for application to these types of terrestrial samples within the Kalahari region, when samples are well preserved.

However, modern to recent pan evaporites yield temperatures that are much lower (9 °C) and therefore we would caution against their use for temperature reconstructions. This is highlighted with the inconsistent results yielded from the older evaporite samples (Table 4). The relatively high $\delta^{18}O_w$ values recorded from the evaporite samples likely reflects intense evaporation and possible kinetic effects.

4.5 Transfer functions for MAAT

In NW Botswana, the modern annual average air temperature is 22 °C (Oromeng et al., 2021). For the modern samples, the transfer function of Hren and Sheldon (2012) yields measured MAAT temperatures that correspond to a MAAT of 21.7 ± 1.9 °C and Terrarez et al. (2025) yields measured MAAT temperatures that correspond to a MAAT of 23.0 ± 1.9 °C. Both transfer functions are therefore within error of the expected annual average air temperature. It should be noted, however, that transfer functions assume a seasonal window during which carbonate formation occurs, meaning that reconstructed temperatures may reflect the conditions prevailing during periods of active carbonate precipitation rather than a strict annual mean. In the semi-arid environment of NW Botswana, carbonate formation is likely associated with periods of increased moisture availability and soil activity, which may bias the signal toward the wetter season. The transfer functions take note of this and the close agreement between the reconstructed values and the observed MAAT suggests that a reasonable approximation of regional temperature conditions is provided. Given the small sample set, we apply the transfer function of Terrarez et al. (2025) in this study as the equation has a reduced error and incorporates latitude and altitude effects, making it more appropriate for this region.

5. Discussion

5.1 Isotope variation in carbonates

The variation in the stable isotope measurements in this study indicates that a primary source of uncertainty in the interpretation of the results is the possible influence of weathering and diagenetic processes. The thin and primarily unconsolidated sedimentary cover enables in-situ weathering of underlying Precambrian basement rocks by bottom-up processes. This is

https://doi.org/10.5194/egusphere-2026-2583
Preprint. Discussion started: 22 May 2026

compounded by the evidence of bioturbation, as well as meteoric influences that gave rise to the various textures observed in the micromorphology (Figure 5). The variations in the isotope geochemistry corroborate the post-depositional interpretations. The greater range in the $\delta^{18}O$ values suggests the predominant influence of surface and groundwater in the precipitation of carbonates (Figure 7). Samples with the lowest $\delta^{13}C$ and $\delta^{18}O$ values are comparable to previous results of Kalahari Group calcretes sampled in a drill core (KPH4), that represents highly recrystallized sparitic calcrete (Figure 8; Linol, 2013). In marlstones closer to the surface, the more enriched $\delta^{13}C$ values are attributed to the influence from the biological components in the overlying soil.

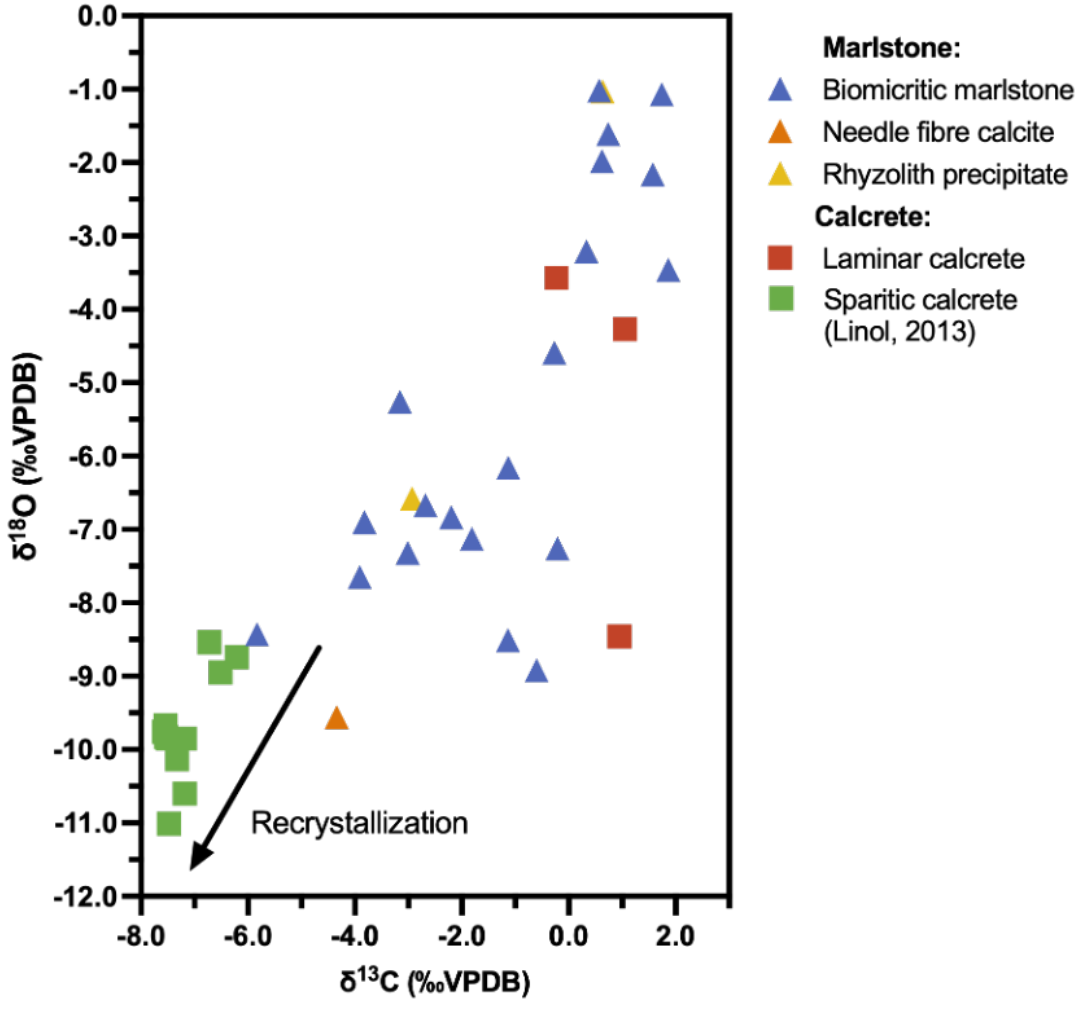

Figure 8: $\delta^{13}C$ versus $\delta^{18}O$ values of measured Kalahari Group sediments and calcretes from Tso1, KGP58, KGP71 and KPH drill cores (see also Linol, 2013). The reworked calcretes, identified by petrographic screening (squares) have relatively lower $\delta^{18}O$ values in comparison to the marlstones (triangles).

The variation in stable isotopes due to weathering is not reflected in the measured Δ_{47} temperatures, and thus secondary carbonate precipitation cannot be interpreted from these values alone. However, it is likely that post-depositional influences

https://doi.org/10.5194/egusphere-2026-2583
Preprint. Discussion started: 22 May 2026

are reflected in the $\delta^{18}O_w$ values calculated from the Δ_{47} temperatures, as there is a clear distinction between samples influenced by present-day meteoric and groundwater (Figure 9; McCarthy et al., 1998).

In soil concretions and Bk horizons, the measured Δ_{47} temperatures are generally warmer than other carbonate types. However, the calculated $\delta^{18}O_w$ value of –6.2 ± 1.2 ‰ VSMOW is comparable to that of the subsurface marlstones influenced by meteoric and groundwater (Figure 9). This is attributed to secondary carbonate precipitation during post-depositional processes. In addition, site-specific factors in soil carbonates complicate the interpretation as surface temperatures, diurnal fluctuations, and the calculated 'damping' depths of soil profiles where the fluctuations of climatic parameters may no longer influence the precipitation of carbonates need to be considered (Breecker et al., 2009; Quade et al., 2013). This is expected from the recent surficial sediments analysed in this study, as they do not record average climate conditions, but rather much warmer temperatures.

In contrast, the $\delta^{18}O$ values in fossil gastropods are distinctively higher (Figure 9), which are comparable with a previous study (Wiese et al., 2020). In addition, paired analyses on a subset of fossil gastropods indicate carbonate precipitation in equilibrium (Table 5). This geochemistry is indicative of primary carbonate precipitates and are thus suitable for paleoclimate reconstructions. Fossil gastropods as a proxy are supported by the ^{14}C ages (Figure 3). Marlstone collected in drill cores from the same depths as these fossils yield differing ages, which can be attributed to the heterogeneous microfabrics exhibited (Figure 7 and Figure 8) and suggests contamination between different carbonate forms during homogenization. However, the recurrent age of ~33 ka for fossil gastropods at similar depths supports relatively good preservation.

https://doi.org/10.5194/egusphere-2026-2583
Preprint. Discussion started: 22 May 2026

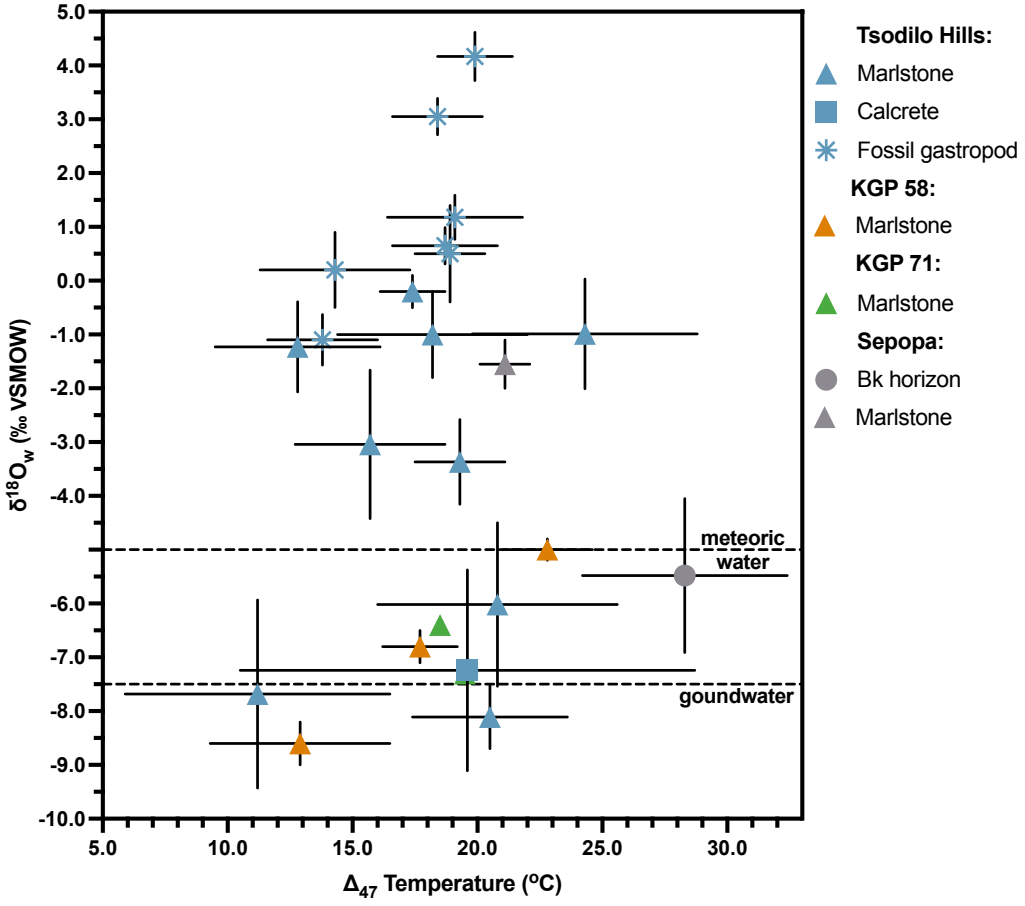

Figure 9: Measured Δ_{47} temperatures of Kalahari Group sediments, calcrete, soil concretions, and fossil gastropods. The samples from outcrops preserve relatively higher δ^{18}Ow values compared to subsurface samples in KGP 58 and KGP 71 drill cores. The meteoric and groundwater lines are from McCarthy et al., 1998.

5.2 Limitations

The multi-proxy approach has identified that not all samples are suitable for paleoclimate reconstructions using clumped isotopes due to the secondary carbonate precipitation and heterogeneity in texture. The most robust results are therefore derived from fossil gastropods of the *Radix* and *Bulinus* species. In this study the dataset is limited for these gastropods, which constrains the broader applicability for global climate model inputs. Despite the limited dataset, these results identify a valuable archive for future investigation and provide initial direct temperature estimates for the interior Kalahari Plateau.

5.3 Paleoclimate significance

Late Pleistocene fossil gastropod shells of the *Radix and Bulinus* species are identified as robust potential archives for paleotemperature and paleohydrology reconstructions. The application of carbonate clumped isotopes on terrestrial snails in

https://doi.org/10.5194/egusphere-2026-2583
Preprint. Discussion started: 22 May 2026

the northern hemisphere has also yielded results that suggest snail are a useful archive (e.g. Bricker et al., 2023). The fossil gastropods that are determined to be best preserved yield an average temperature of 17.6 ºC (Figure 10), which corresponds to a MAAT of ~15 ºC. The reconstructed temperature is several degrees lower than the modern mean annual air temperature of ~22 °C in northwest Botswana, suggesting cooler climatic conditions across the Kalahari Plateau during this interval in comparison to the present (Figure 1). These cooler conditions are comparable with results from other parts of southern Africa. Speleothem-based paleotemperature reconstructions from the Cango Caves indicate cooler conditions during the Late Pleistocene relative to the present, with temperature estimates several degrees lower than modern values (Talma and Vogel, 1992). Similarly, sedimentary and geochemical records from Tswaing Crater Lake suggest substantial climatic variability during the Late Pleistocene, including cooler intervals associated with changes in hydrological balance and regional circulation patterns (Kristen, 2007). Although these archives represent different depositional environments and are located outside the Kalahari Basin, the broadly cooler conditions inferred from these studies are consistent with the lower mean annual air temperatures reconstructed here from fossil gastropods.

The Kalahari Plateau remains underrepresented in regional paleoclimate datasets, and the fossil gastropods identified in this study provide a promising archive for future more extensive quantitative temperature reconstructions. Integrating these records with other regional archives and global climate model simulations will help clarify the spatial patterns and drivers of Late Pleistocene climate variability in southern Africa and aid in increasing the accuracy of global climate models.

https://doi.org/10.5194/egusphere-2026-2583
Preprint. Discussion started: 22 May 2026

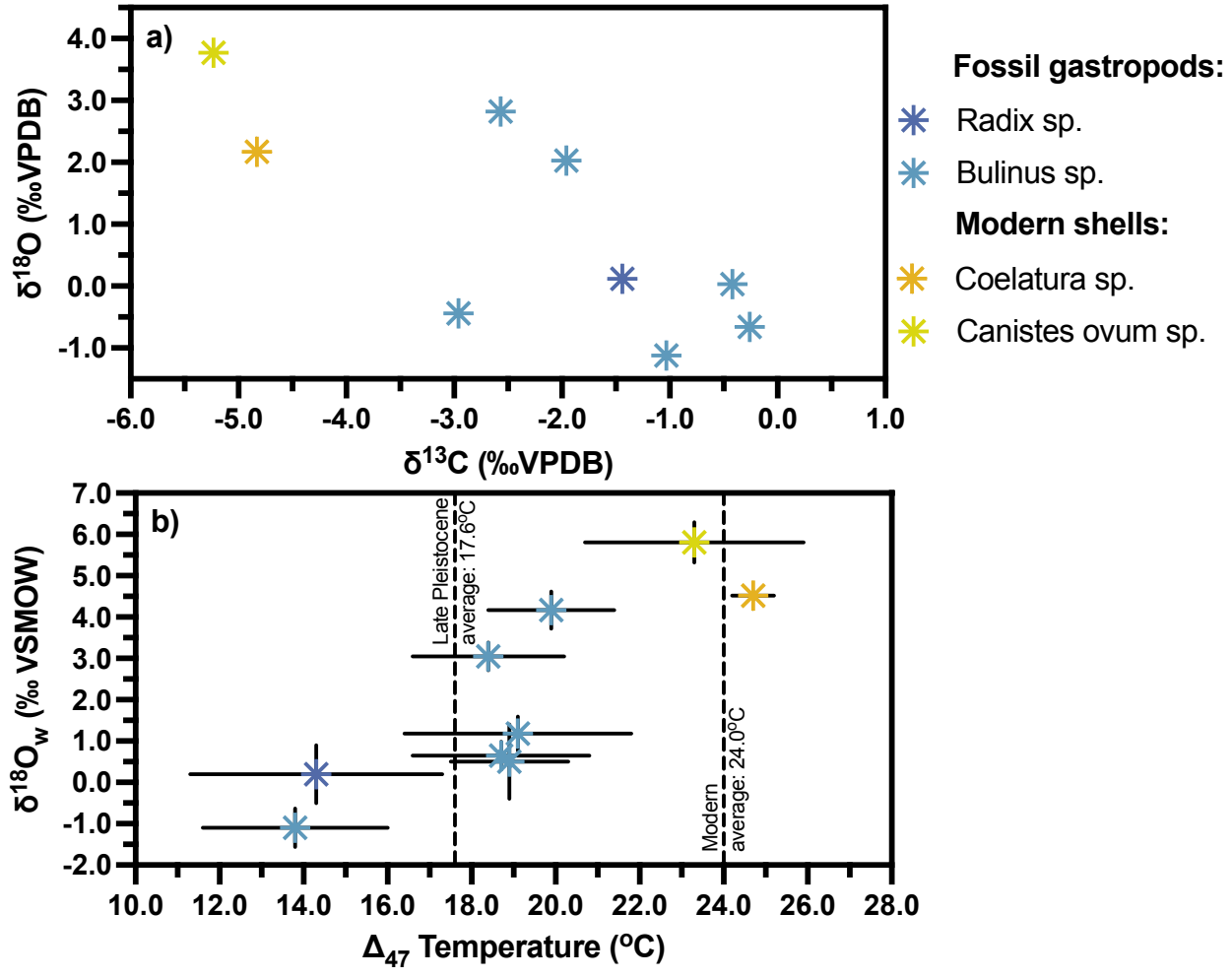

Figure 10: C and O stable and clumped isotope results of modern and fossil shells from the Kalahari Group. a) The depleted $\delta^{18}O$ value suggests incorporation of the sediment matrix in the analysis. The difference in the $\delta^{13}C$ values between the modern and fossil carbonates is attributed to the influence of organic matter in the river channels from C_4 and C_3 vegetation and loss of aquatic dissolved inorganic carbon (Meier et al., 2015), where the modern samples were collected; b) The measured Δ_{47} temperatures are distinctively lower in the fossil gastropods compared to the modern mussel and snail.

6. Conclusion

This study aimed to identify a suitable archive for climate reconstructions from the carbonates preserved in the Kalahari Group sediments. The multi-proxy approach applied to the study of carbonates from the Kalahari Group sediments has identified well-preserved, late Pleistocene fossil gastropod shells as reliable archives for reconstructing quantitative temperature in southern Africa. The results of this study will contribute to resolving the conflicting interpretations regarding the driving forces

https://doi.org/10.5194/egusphere-2026-2583
Preprint. Discussion started: 22 May 2026

behind the late Quaternary climate of southern Africa, which have been long hampered by the lack of quantitative temperature estimates.

Despite the limited number of samples, our temperature reconstructions from the gastropod shells revealed an average mean annual air temperature of ~15 ºC between 32.52 ± 0.35 ka and 34.53 ± 0.35 ka, suggesting cooler conditions during the Late Pleistocene. Future work should focus on obtaining additional direct temperature estimates from fossil gastropods within the Kalahari region, as well as integrating these results with paleoclimate records, including speleothem archives from the Cango Caves and lake sediments from Tswaing Crater, in South Africa as well as lake sediments from the Makgadikgadi Lakes (Kahsay et al., 2026). Expanding such datasets will help refine regional paleotemperature reconstructions and improve our understanding of the mechanisms driving Late Pleistocene climate variability in southern Africa. Additionally, in a global context this is essential in narrowing the gap in climate models that are biased towards the northern hemisphere.

Appendix A

Table A 1: Summary of sample location, descriptions and analyses conducted.

Locality	Sample name	Elevation (masl)	Latitude	Longitude	Depth (m)	Description	Analysis conducted
Tsodilo Hills							
	Tso1_a	1007	-18.78277778	21.71972222	0.2	Fossiliferous white marlstone	Δ_{47}, $\delta^{13}C$ and $\delta^{18}O$
	Tso1_b	1003,5	-18.78277778	21.71972222	3.5	Fossiliferous white marlstone with sandy infill	Δ_{47}, $\delta^{13}C$ and $\delta^{18}O$
	Tso1_c	1003,5	-18.78277778	21.71972222	3.5	Fossiliferous white marlstone with sandy infill	$\delta^{13}C$ and $\delta^{18}O$
	Tso1_d	1001,4	-18.78277778	21.71972222	5.6	Fossiliferous white marlstone. Quartz pebbles	Δ_{47}, $\delta^{13}C$ and $\delta^{18}O$
	01_a	1000	-18.794063	21.738049	outcrop	Laminar calcrete cap	Δ_{47}, $\delta^{13}C$ and $\delta^{18}O$
	01_b	1000	-18.794063	21.738049	outcrop	Biomicritic grey marlstone.	Δ_{47}, $\delta^{13}C$ and $\delta^{18}O$
	01_c	1000	-18.794063	21.738049	outcrop	Biomicritic grey diatomaceous marlstone.	Δ_{47}, $\delta^{13}C$ and $\delta^{18}O$
	02_a	1008	-18.793039	21.73041	outcrop	Grey marlstone. Rhyzolith precipitate.	Δ_{47}, $\delta^{13}C$ and $\delta^{18}O$
	02_b	1008	-18.793039	21.73041	outcrop	Biomicritic grey marlstone.	Δ_{47}, $\delta^{13}C$ and $\delta^{18}O$
	02_c	1008	-18.793039	21.73041	outcrop	Laminar calcrete cap.	$\delta^{13}C$ and $\delta^{18}O$
	02_d	1008	-18.793039	21.73041	outcrop	Laminar calcrete cap.	$\delta^{13}C$ and $\delta^{18}O$
	02_e	1008	-18.793039	21.73041	outcrop	Biomicritic grey marlstone.	$\delta^{13}C$ and $\delta^{18}O$
	03_a	1003	-18.794089	21.736374	outcrop	Grey-white marlstone. Chalky textured reprecipitated needle-fibre calcite with muddy infill.	Δ_{47}, $\delta^{13}C$ and $\delta^{18}O$
	03_b	1003	-18.794089	21.736374	outcrop	Biomicritic grey marlstone.	Δ_{47}, $\delta^{13}C$ and $\delta^{18}O$

03_c	1003	-18.794089	21.736374	outcrop	Biomicritic grey marlstone.	$\delta^{13}C$ and $\delta^{18}O$
03sn_d	1003	-18.794089	21.736374	outcrop	Fossil gastropod. *Bulinus sp.*	$\delta^{13}C$ and $\delta^{18}O$
03sn_a	1003	-18.794089	21.736374	outcrop	Fossil gastropod. *Radix sp.*	Δ_{47}, $\delta^{13}C$ and $\delta^{18}O$
03sn_b	1003	-18.794089	21.736374	outcrop	Fossil gastropod. *Bulinus sp.*	Δ_{47}, $\delta^{13}C$ and $\delta^{18}O$
03sn_c	1003	-18.794089	21.736374	outcrop	Fossil gastropod. *Bulinus sp.*	Δ_{47}, $\delta^{13}C$ and $\delta^{18}O$
03sn_e	1003	-18.794089	21.736374	outcrop	Fossil gastropod. Bulinus sp.	Δ_{47}, Δ_{48}, $\delta^{13}C$ and $\delta^{18}O$
03sn_f	1003	-18.794089	21.736374	outcrop	Fossil gastropod. *Bulinus sp.*	Δ_{47}, Δ_{48}, $\delta^{13}C$ and $\delta^{18}O$
03sn_g	1003	-18.794089	21.736374	outcrop	Fossil gastropod. *Bulinus sp.*	Δ_{47}, Δ_{48}, $\delta^{13}C$ and $\delta^{18}O$
03sn_h	1003	-18.794089	21.736374	outcrop	Fossil gastropod. *Bulinus sp.*	Δ_{47}, Δ_{48}, $\delta^{13}C$ and $\delta^{18}O$
Shakawe						
KGP58_a	1009	-18.487759	21.87189	4	Carbonate concretion from an interpreted Bk Horizon.	$\delta^{13}C$ and $\delta^{18}O$
KGP58_b	1009	-18.487759	21.87189	4	White calcic sand from an interpreted Bk Horizon.	$\delta^{13}C$ and $\delta^{18}O$
KGP58_c	1005	-18.487759	21.87189	8.3	Biomicritic grey marlstone. Bioturbated	$\delta^{13}C$ and $\delta^{18}O$
KGP58_d	1005	-18.487759	21.87189	8.3	Laminar calcrete cap.	$\delta^{13}C$ and $\delta^{18}O$
KGP58_e	1005	-18.487759	21.87189	8.3	Biomicritic grey marlstone. Bioturbated.	Δ_{47}, $\delta^{13}C$ and $\delta^{18}O$
KGP58_f	1002	-18.487759	21.87189	11	Biomicritic grey marlstone.	Δ_{47}, $\delta^{13}C$ and $\delta^{18}O$
KGP58_g	1002	-18.487759	21.87189	11	Biomicritic grey marlstone.	$\delta^{13}C$ and $\delta^{18}O$
KGP58sn_b	1002	-18.487759	21.87189	11	Fossil gastropod (matrix not completely removed)	$\delta^{13}C$ and $\delta^{18}O$

	KGP58_h	990	-18.487759	21.87189	23	Fossiliferous marlstone.	Δ_{47}, $\delta^{13}C$ and $\delta^{18}O$
	KGP71_a	988	-18.501881	21.938589	4.5	Biomicritic grey-white marlstone.	Δ_{47}, $\delta^{13}C$ and $\delta^{18}O$
	KGP71_b	992,5	-18.501881	21.938589	4.5	Biomicritic grey-white marlstone.	Δ_{47}, $\delta^{13}C$ and $\delta^{18}O$
	KGP71_c	986	-18.501881	21.938589	5.5	Biomicritic grey-white marlstone.	Δ_{47}, $\delta^{13}C$ and $\delta^{18}O$
	KGP71_d	986	-18.501881	21.938589	5.5	Biomicritic grey-white marlstone.	Δ_{47}, $\delta^{13}C$ and $\delta^{18}O$
	KGP71_e	991,5	-18.501881	21.938589	5.5	Biomicritic grey-white marlstone.	Δ_{47}, $\delta^{13}C$ and $\delta^{18}O$
Sepopa							
	04_a	994	-18.73280753	22.12561667	outcrop	Biomicritic grey marlstone	Δ_{47}, $\delta^{13}C$ and $\delta^{18}O$
	04_b	994	-18.73280753	22.12561667	outcrop	Biomicritic grey marlstone.	$\delta^{13}C$ and $\delta^{18}O$
	05_c	989	-18.74356858	22.167158	outcrop	Nodular carbonate concretion. Bk horizon.	Δ_{47}, $\delta^{13}C$ and $\delta^{18}O$
Lake Ngami							
	Nga2_a	921	-20.49416667	22.72888889	3-4	Sandy marl	Δ_{47}, $\delta^{13}C$ and $\delta^{18}O$
	Nga2_b	913	-20.49416667	22.72888889	11-12	Sandy marl	Δ_{47}, $\delta^{13}C$ and $\delta^{18}O$
	Nga2_c	881	-20.49416667	22.72888889	43-44	Sandy marl	Δ_{47}, $\delta^{13}C$ and $\delta^{18}O$
	Nga2_d	839	-20.49416667	22.72888889	85-86	Sandy marl	Δ_{47}, $\delta^{13}C$ and $\delta^{18}O$
	Nga2_e	818	-20.49416667	22.72888889	106-107	Sandy marl	Δ_{47}, $\delta^{13}C$ and $\delta^{18}O$
	Nga2_f	806	-20.49416667	22.72888889	118-119	Sandy marl	Δ_{47}, $\delta^{13}C$ and $\delta^{18}O$
Maun							
	06_a	944	-19.943291	23.488534	surface	Modern freshwater mussel from the Thamalakane River. *Coelatura sp.*	Δ_{47}, $\delta^{13}C$ and $\delta^{18}O$

	06_b	944	-19.943291	23.488534	surface	Modern freshwater snail from the Thamalakane River. *Canistes ovum sp.*	Δ_{47}, $\delta^{13}C$ and $\delta^{18}O$
Kang							
	Ka_e	1122	-23.698996	22.802468	0.85-1	Muddy grey pan evaporites.	$\delta^{13}C$ and $\delta^{18}O$
	Ka_c	1122	-23.698996	22.802468	0.4-0.8	Muddy grey pan evaporites.	$\delta^{13}C$ and $\delta^{18}O$
	Ka_a	1122	-23.698996	22.802468	0-0.4	Muddy grey pan evaporites.	Δ_{47}, $\delta^{13}C$ and $\delta^{18}O$
	Ka_b	1122	-23.698996	22.802468	0.4-0.8	Muddy grey pan evaporites.	Δ_{47}, $\delta^{13}C$ and $\delta^{18}O$
	Ka_d	1122	-23.698996	22.802468	0.8-1	Muddy grey pan evaporites.	Δ_{47}, $\delta^{13}C$ and $\delta^{18}O$
Barberspan							
	07_a	1331	-26.589858	25.603467	surface	Surficial sandy grey marl.	Δ_{47}, $\delta^{13}C$ and $\delta^{18}O$

https://doi.org/10.5194/egusphere-2026-2583
Preprint. Discussion started: 22 May 2026

Data availability

All geochemistry data described in this paper are included in tables 2, 3, 4 and 5.

Author contributions

S.M performed fieldwork, analytical work (petrography and clumped isotope analysis), data interpretation, data visualisation and original manuscript writing. D.U conducted clumped isotope analysis and contributed to data interpretation and data visualization, and original manuscript writing. A.A contributed to data interpretation, data visualisation and original manuscript writing. J.L contributed to data interpretation and original manuscript writing. B.L contributed to fieldwork, data interpretation, and manuscript editing. D.G contributed to data interpretation and editing the manuscript. A.A contributed to data interpretation and manuscript writing. A.T contributed to data interpretation, data visualisation and manuscript editing.

Acknowledgments

We acknowledge Tsodilo Resources for allowing us access to their drill cores and for hosting us for 3 weeks in Botswana to conduct fieldwork. We further acknowledge the aid of Wille Deysel in the Department for Geoscience at Nelson Mandela University for assisting with thin section preparation. We acknowledge the lab manager at UCLA, Ben Arnold, for conducting the clumped isotope analysis.

Financial Support

This research was supported by several funding bodies. We acknowledge financial support from the National Research Foundation (NRF), through AEON, which funded fieldwork, thin section preparation, stable carbon and oxygen isotope analyses and partially supported a research visit to UCLA for further analyses. We acknowledge UCLA CDLS, through the Waverly Street Foundation and Packard Foundation, for supporting the research visit and the radiocarbon and clumped isotope analyses. Lastly, we acknowledge the Council for Geoscience for their financial support. This is AEON Publication number 226 and Iphakade Publication number 299.

References

Affek, H. P. and Eiler, J. M.: Abundance of mass 47 CO_2 in urban air, car exhaust, and human breath, Geochim. Cosmochim. Acta, 70, 1–12, https://doi.org/10.1016/j.gca.2005.08.021, 2006.

https://doi.org/10.5194/egusphere-2026-2583
Preprint. Discussion started: 22 May 2026

Bajnai, D., Guo, W., Spotl, C., Coplen, T. B., Methner, K., Löffler, N., Krsnik, E., Gischler, E., Hansen, M., Henkel, D., Price, G. D., Raddatz, J., Scholz, D., Fiebig, J.: Dual clumped isotope thermometry resolves kinetic biases in carbonate formation temperatures, Nat Commun, 11, 4005, https://doi.org/10.1038/s41467-020-17501-0, 2020.

Bernasconi, S. M., Muller, I. A., Bergmann, K. D., Breitenbach, S. F. M., Fernandez, A., Hodell, D. A., Jaggi, M., Meckler, A. N., Millian, I., Zieglar, M.: Reducing Uncertainties in Carbonate Clumped Isotope Analysis Through Consistent Carbonate-Based Standardization, Geochem. Geophys. Geosyst. 19, 2895–2914, https://doi.org/10.1029/2017GC007385, 2018.

Bernasconi, S., Daëron, M., Bergmann, K., Bonifacie, M., Meckler, A., Affek, H., Anderson, N, Bajnai, D., Barkan, E., Beverly, E., Blamart, D., Burgener, L., Calmels, D., Chaduteau, C., Clog, M., Davidheiser-Kroll, B., Davies, A., Dux, F., Eiler, J., Elliott, B., Fetrow, A., Fiebig, J., Goldberg, S., Hermoso, M., Huntington, K., Hyland, E., Ingalls, M., Jaggi, M., John, C., Jost, A., Katz, S., Kelson, J., Kluge, T., Kocken, I., Laskar, A., Leutert, T., Liang, D., Lucarelli, J., Mackey, T., Mangenot, X., Meinicke, N., Modestou, S., Muller, I., Murray, S., Neary, A., Packard, N., Passey, B., Pelletier, E., Petersen, S., Piasecki, A., Schauer, A., Snell, K.E., Swart, P., Tripati, A., Upadhyay, D., Vennemann, T., Winkelstern, I., Yarian, D., Yoshida, N., Zhang, N., and Ziegler, M.: InterCarb: A Community Effort to Improve Interlaboratory Standardization of the Carbonate Clumped Isotope Thermometer Using Carbonate Standards, Geochem. Geophy. Geosy. 22, e2020GC009588, https://doi.org/10.1029/2020GC009588, 2021.

Brand, W. A., Assonov, S. S., & Coplen, T. B.: Correction for the O-17 interference in delta (C-13) measurements when analyzing CO_2 with stable isotope mass spectrometry (IUPAC Technical Report). Pure. Appl. Chem., 82, 1719–1733. https://doi.org/10.1351/PAC-REP-09-01-05, 2010.

Brook, G. A., Railsback, L. B. and Marais, E.: Reassessment of carbonate ages by dating both carbonate and organic material from an Etosha Pan (Namibia) stromatolite: evidence of humid phases during the last 20 ka, Quat. Int., 229, 24–37, https://doi.org/10.1016/j.quaint.2009.09.031, 2011.

Breecker, D., Sharp, Z. and McFadden, L. D.: Seasonal bias in the formation and stable isotopic composition of pedogenic carbonate in modern soils from central New Mexico, USA, Geol. Soc. Am. Bull., 121, 630–640, https://doi.org/10.1130/B26413.1, 2009.

Bricker, H. L., Bateman, J. B., Elliott, B., Mitsunaga, B. A., Mering, J., Foster, I. S., Yanes, Y., Oches, E. A., Eagle, R. A., and Tripati, A. K.: A multi-region study of carbonate clumped isotope data from terrestrial snails, Palaeogeogr. Palaeoclimatol. Palaeoecol., 628, 111754, https://doi.org/10.1016/j.palaeo.2023.111754, 2023

Burrough, S. L., Thomas, D. S. G. and Bailey, R. M.: Mega-Lake in the Kalahari: a Late Pleistocene record of the Palaeolake Makgadikgadi system, Quat. Sci. Rev., 28, 1392–1411, https://doi.org/10.1016/j.quascirev.2009.02.007, 2009.

Burrough, S. L., Thomas, D. S. G., Shaw, P. A. and Bailey, R. M.: Multiphase Quaternary highstands at Lake Ngami, Kalahari, northern Botswana, Palaeogeogr. Palaeoclimatol. Palaeoecol., 253, 280–299, https://doi.org/10.1016/j.palaeo.2007.06.008, 2007.

Chase, B., Harris, C., De Wit, M. J., Kramers, J., Doel, S. and Stankiewicz, J.: South African speleothems reveal influence of high- and low-latitude forcing over the past 113.5 kyr, Geology, 49, 1353–1357, https://doi.org/10.1130/G49323.1, 2021.

https://doi.org/10.5194/egusphere-2026-2583
Preprint. Discussion started: 22 May 2026

Cooke, H. J.: Landform evolution in the context of climatic change and neo-tectonism in the Middle Kalahari of north-central Botswana, Trans. Inst. Br. Geogr., 5, 80–99, https://doi.org/10.2307/622100 ,1980.

Cordova, C. E., Scott, L., Chase, B. M. and Chevalier, M.: Late Pleistocene–Holocene vegetation and climate change in the middle Kalahari, Lake Ngami, Botswana, Quat. Sci. Rev., 171, 199–215, https://doi.org/10.1016/j.quascirev.2017.07.004, 2017.

Defliese, W. F., & Tripati, A.: Analytical effects on clumped isotope thermometry: Comparison of a common sample set analyzed using multiple instruments, types of standards, and standardization windows. Rapid Commun. Mass Spectrom., 34, e8666. https://doi.org/10.1002/rcm.8666, 2020.

Dennis, K. J., Affek, H. P., Passey, B. H., Schrag, D. P., & Eiler, J. M.: Defining an absolute reference frame for 'clumped'isotope studies of CO2. Geochim. Cosmochim. Acta., 75, 7117-7131, https://doi.org/10.1016/j.gca.2011.09.025 2011.

de Wit, M.: The Kalahari Epeirogeny and climate change: differentiating cause and effect from core to space, S. Afr. J. Geol., 110, 367–392, https://doi.org/10.2113/gssajg, 2007.

de Wit, M. C. J., Haddon, I. G., and Robey, J. V. A.: The Nxaunxau kimberlites of northwest Botswana, 11th Int. Kimberlite Conf., Extended Abstracts, 2017.

Doucouré, C. M. and De Wit, M. J.: Old inherited origin for the present near-bimodal topography of Africa, J. Afr. Earth Sci., 36, 371–388, https://doi.org/10.1016/S0899-5362(03)00019-8, 2003.

Eiler, J. M.: "Clumped-isotope" geochemistry—The study of naturally occurring multiply substituted isotopologues, Earth Planet. Sci. Lett., 262, 309–327, https://doi.org/10.1016/j.epsl.2007.08.020, 2007.

Fiebig, J., Bajnai, D., Guo, W., Henkes, G., Passey, B. H., Tripati, A., Eagle, R., Schauble, E. A. and Eiler, J. M.: Calibration of the dual clumped isotope thermometer for carbonates, Geochim. Cosmochim. Acta., 245, 1–15, https://doi.org/10.1016/j.gca.2018.10.042, 2019.

Fiebig, J., Daeron, M., Bernecker, M., Guo, W., Schneider, G., Boch., Bernasconi, S. M., Jautzy, J., Dietzel, M.: Calibration of the dual clumped isotope thermometer for carbonates, Geochim. Cosmochim. Acta., 312, 235-256, https://doi.org/10.1016/j.gca.2021.07.012, 2021.

Geppert, M., Riedel, F., Gummersbach, V. S., Gutjahr, S., Hoelzmann, P., Reyes Garzón, M. D., Shemang, E. M. and Hartmann, K.: Late Pleistocene hydrological settings at world heritage Tsodilo Hills (NW Kalahari, Botswana), a site of ancient human occupation, Quat. Sci. Adv., 3, 100022, https://doi.org/10.1016/j.qsa.2021.100022, 2021.

Ghosh, P., Adkins, J., Affek, H., Balta, B., Guo, W., Schauble, E. A., Schrag, D. and Eiler, J. M.: 13C–18O bonds in carbonate minerals: a new kind of paleothermometer, Geochim. Cosmochim. Acta., 70, 1439–1456, https://doi.org/10.1016/j.gca.2005.11.014, 2006.

Gumbricht, T., McCarthy, T. and Merry, C. L.: The topography of the Okavango Delta, Botswana, and its tectonic and sedimentological implications, S. Afr. J. Geol., 104, 243–264, https://doi.org/10.2113/104.3.243, 2001.

https://doi.org/10.5194/egusphere-2026-2583
Preprint. Discussion started: 22 May 2026

Haddon, I. G.: The Sub-Kalahari geology and tectonic evolution of the Kalahari Basin, PhD thesis, University of the Witwatersrand, Johannesburg, South Africa, 2005.

Haddon, I. and McCarthy, T.: The Mesozoic–Cenozoic interior sag basins of Central Africa: the Late Cretaceous–Cenozoic Kalahari and Okavango basins, J. Afr. Earth Sci., 43, 316–333, https://doi.org/10.1016/j.jafrearsci.2005.07.008, 2005.

Heiri, O., Lotter, A. F., and Lemcke, G.: Loss on ignition as a method for estimating organic and carbonate content in sediments: reproducibility and comparability of results, J. Paleolimnol., 25, 101–110, doi:10.1023/A:1008119611481, 2001.

Hren, M. T. and Sheldon, N. D.: Temporal variations in lake water temperature: paleoenvironmental implications of lake carbonate $\delta^{18}O$ and temperature records, Earth Planet. Sci. Lett., 337–338, 77–84, https://doi.org/10.1016/j.epsl.2012.05.034, 2012.

Huntsman-Mapila, P., Ringrose, S., Mackay, A.W., Downey, W.S., Modisi, M., Coetzee, S.H., Tiercelin, J.J., Kampunzu, A.B. and Vanderpost, C.: Use of the geochemical and biological sedimentary record in establishing palaeo-environments and climate change in the Lake Ngami basin, NW Botswana. Quat. Int., 148, 51-64, https://doi.org/10.1016/j.quaint.2005.11.029, 2006.

John, C. M., and Bowen, D.: Community software for challenging isotope analysis: First applications of 'Easotope' to clumped isotopes, Rapid Commun Mass Spectrom., 30, 2285-2300, https://www.dx.doi.org/10.1002/rcm.7720, 2016.

Jouzel, J., Masson-Delmotte, V., Cattani, O., Dreyfus, G., Falourd, S., Hoffmann, G., Minster, B., Nouet, J., Barnola, J.M., Chappellaz, J. and Fischer, H.: Orbital and millennial Antarctic climate variability over the past 800,000 years, Science, 317, 793-796, 10.1126/science.1141038, 2007.

Kahsay, T., Asrat, A., Sinha, N., Marchegiano, M., and Franchi, F.: Late Pleistocene to Holocene Multi-proxy Paleoenvironmental and Paleoclimatic Reconstruction of the Makgadikgadi Basin, Central Kalahari, Botswana, EGU General Assembly 2026, Vienna, Austria, 3–8 May 2026, EGU26-7064, https://doi.org/10.5194/egusphere-egu26-7064, 2026

King, L. C.: South African scenery: a textbook of geomorphology, Oliver and Boyd, Edinburgh, 308 pp., 1963.

Kristen, I., Fuhrmann, A., Thorpe, J., Rohl, U., Wilkes, H., and Oberhansli, H.: Hydrological changes in southern Africa over the last 200 Ka as recorded in lake sediments from the Tswaing impact crater, S. Afr. J. Geol., 110, 311-326, https://doi.org/10.2113/gssajg.110.2-3.311, 2007.

Linol, B.: Sedimentology and sequence stratigraphy of the Congo and Kalahari basins of south Central Africa and their evolution during the formation and break-up of west Gondwana, PhD thesis, Nelson Mandela University, https://doi.org/10.13140/RG.2.2.11671.57767, 2013.

Linol, B., De Wit, M. J., Guillocheau, F., De Wit, M. C., Anka, Z. and Colin, J.-P.: Formation and collapse of the Kalahari duricrust ("African Surface") across the Congo Basin, with implications for changes in rates of Cenozoic offshore sedimentation, in: Geology and Resource Potential of the Congo Basin, Springer, Berlin, 193–210, https://doi.org/10.1007/978-3-642-29482-2_11, 2015.

https://doi.org/10.5194/egusphere-2026-2583
Preprint. Discussion started: 22 May 2026

Lucarelli, J. K., Carroll, H. M., Ulrich, R. N., Elliott, B. M., Coplen, T. B., Eagle, R. A. and Tripati, A. K.: Equilibrated gas and carbonate standard-derived dual (Δ47 and Δ48) clumped isotope values, Geochem. Geophys. Geosyst., 24, e2022GC010458, https://doi.org/10.1029/2022GC010458, 2023a.

Lucarelli, J. K., Purgstaller, B., Ulrich, R. N., Parvez, Z., Leis, A., Goetschl, K. E., Eagle, R. A., Dietzel, M. and Tripati, A. K.: Dual clumped (Δ47–Δ48) isotope data for amorphous carbonates and transformation products reveal a novel mechanism for disequilibrium clumped isotope effects, Geochim. Cosmochim. Acta, 359, 1–17, https://doi.org/10.1016/j.gca.2023.07.027, 2023b.

Lucarelli, J., Purgstaller, B., Parvez, Z., Watkins, J.M., Eagle, R.A., Dietzel, M. and Tripati, A., 2025. Dual clumped isotope (Δ47, Δ48) values for calcite grown at varying pH and carbonic anhydrase concentrations constrain equilibrium and kinetic isotope effects. Geochem. Geophys. Geosyst., 26, e2025GC012202, https://doi.org/10.1029/2025GC012202, 2025.

Lutjeharms, J. R. E.: The ocean environment off southeastern Africa: a review, S. Afr. J. Sci., 102, 419-426, https://hdl.handle.net/10520/EJC96603, 2006.

Marret, F., de Vernal, A., Benderra, F. and Harland, R.: Late Quaternary sea-surface conditions at DSDP Hole 594 in the southwest Pacific Ocean based on dinoflagellate cyst assemblages. J. Quaternary Sci., 16, 739-751. https://doi.org/10.1002/jqs.648, 2001.

McCarthy, T. S., Bloem, A., & Larkin, P. A.: Observations on the hydrology and geohydrology of the Okavango Delta. S. Afr. J. Geol., 101, 101-117, https://hdl.handle.net/10520/EJC-1abed244bb, 1998.

Modisi, M. P., Atekwana, E. A., Kampunzu, A. and Ngwisanyi, T. H.: Rift kinematics during the incipient stages of continental extension: evidence from the nascent Okavango Rift Basin, northwest Botswana, Geology, 28, 939–942, https://doi.org/10.1130/0091-7613(2000)28<939:RKTISS>2.0.CO;2, 2000.

Musa, S.: The application of carbonate clumped isotope geochemistry to paleoclimates reconstruction in south-central Africa, MSc thesis, Nelson Mandela University, http://hdl.handle.net/10948/2042280

Nicholson, S. E., Some, B, Kone, B.:An Analysis of Recent Rainfall Conditions in West Africa, Including the Rainy Seasons of the 1997 El Nin˜o and the 1998 La Nin˜a Years, J. Clim., 13, 2628-2640, https://doi.org/10.1175/1520-0442(2000)013<2628:AAORRC>2.0.CO;2, 2000.

Oromeng, K. V., Atekwana, E. A., Molwalefhe, L. and Ramatlapeng, G. J.: Time-series variability of solute transport and processes in rivers in semi-arid endorheic basins: the Okavango Delta, Botswana, Sci. Total Environ., 759, 143574, https://doi.org/10.1016/j.scitotenv.2020.143574, 2021.

Partridge, T. C., Avery, D. M., Botha, G. A., Brink, J. S., Deacon, J., Herbert, R. S., Maud, R. R., Scholtz, A., Scott, L., Talma, A. S. and Vogel, J. C.: Late Pleistocene and Holocene climatic change in southern Africa, S. Afr. J. Sci., 86, 302–306, 1990.

Partridge, T. C., Demenocal, P. B., Lorentz, S. A., Paiker, M. J., & Vogel, J. C.: Orbital forcing of climate over South Africa: a 200,000-year rainfall record from the Pretoria Saltpan. Quat. Sci. Rev., 16, 1125-1133, https://doi.org/10.1016/S0277-3791(97)00005-X, 1997.

Passarge, S.: Die Kalahari, Vol. 1, Ripol Klassik, Moscow, 1904.

https://doi.org/10.5194/egusphere-2026-2583
Preprint. Discussion started: 22 May 2026

Passey, B. H., Levin, N. E., Cerling, T. E., Brown, F. H., and Eiler, J. M.: High-temperature environments of human evolution in East Africa based on bond ordering in paleosol carbonates, P. Natl. Acad. Sci. USA, 107, 11245–11249, https://doi.org/10.1073/pnas.1001824107, 2010.

Powers, L. A., Johnson, T. C., Werne, J. P., Castañeda, I. S., Hopmans, E. C., Sinninghe Damsté, J. S. and Schouten, S.: Large temperature variability in the southern African tropics since the Last Glacial Maximum, Geophys. Res. Lett., 32, L08706, https://doi.org/10.1029/2004GL022014, 2005.

Quade, J., Eiler, J., Daëron, M. and Achyuthan, H.: The clumped isotope geothermometer in soil and paleosol carbonate, Geochim. Cosmochim. Acta., 105, 92–107, https://doi.org/10.1016/j.gca.2012.11.031, 2013.

Riedel, F., Henderson, A.C.G., Heußner, K., Kaufmann, H. G., Kossler, A., Leipe, C., Shemang E., Taft, L.: Dynamics of a Kalahari long-lived mega-lake system: hydromorphological and limnological changes in the Makgadikgadi Basin (Botswana) during the terminal 50 ka. Hydrobiologia, **739**, 25–53, https://doi.org/10.1007/s10750-013-1647-x, 2014.

Ringrose, S., Harris, C., Huntsman-Mapila, P., Vink, B., Diskins, S., Vanderpost, C. and Matheson, W.: Origins of strandline duricrusts around the Makgadikgadi Pans (Botswana Kalahari) as deduced from their chemical and isotope composition, Sediment. Geol., 219, 262–279, https://doi.org/10.1016/j.sedgeo.2009.05.021, 2009.

Robbins, L., Murphy, M., Stevens, N., Brook, G., Ivester, A., Haberyan, K., Klein, R., Milo, R., Stewart, K. and Matthiesen, D.: Paleoenvironment and archaeology of Drotsky's Cave: western Kalahari Desert, Botswana, J. Archaeol. Sci., 23, 7–22, https://doi.org/10.1006/jasc.1996.0002, 1996.

Shackleton, N. J., Backman, J., Zimmerman, H., Kent, D. V., Hall, M., Roberts, D. G., Schnitker, D., Baldauf, J., Desprairies, A. and Homrighausen, R.: Oxygen isotope calibration of the onset of ice-rafting and history of glaciation in the North Atlantic region, Nature, 307, 620–623, https://doi.org/10.1038/307620a0, 1984.

Shaw, P.: The Desiccation of Lake Ngami: An Historical Perspective, Geogr. J., 151, 318-326, https://doi.org/10.2307/633012, 1985.

Shaw, P. and Cooke, H.: Geomorphic evidence for the Late Quaternary palaeoclimates of the middle Kalahari of northern Botswana, Catena, 13, 349–359, https://doi.org/10.1016/0341-8162(86)90009-3, 1986.

Stuiver, M. and Polach, H. A.: Discussion Reporting of 14C Data, Radiocarbon, 19, 355–363, https://doi.org/10.1017/S0033822200003672, 1977.

Talma, A. S. and Vogel, J. C.: Late Quaternary paleotemperatures derived from a speleothem from Cango Caves, Cape Province, South Africa, Quat. Res., 37, 203–213, https://doi.org/10.1016/0033-5894(92)90040-T, 1992.

Terrazas, A., Hwangbo, N., Arnold, A. J., Ulrich, R. N., and Tripati, A.: Seasonal lake-to-air temperature transfer functions derived from an analysis of 1395 modern lakes: A tool for reconstructing air temperature from proxy-derived lake water temperature, Depos. Rec.,11, 718-738, 10.1002/dep2.326, 2025.

Thackeray, J. F.: Temperature indices from Late Quaternary sequences in South Africa: comparisons with the Vostok core, S. Afr. Geogr. J., 72, 47–49, https://doi.org/10.1080/03736245.1990.10559986, 1990.

https://doi.org/10.5194/egusphere-2026-2583
Preprint. Discussion started: 22 May 2026

Thomas, D. S. G., Brook, G., Shaw, P., Bateman, M., Haberyan, K., Appleton, C., Nash, D., McLaren, S. and Davies, F.: Late Pleistocene wetting and drying in the NW Kalahari: an integrated study from the Tsodilo Hills, Botswana, Quat. Int., 104, 53–67, https://doi.org/10.1016/S1040-6182(02)00125-8, 2003.

Thomas, D. S. G. and Burrough, S. L.: Luminescence-based dune chronologies in southern Africa: analysis and interpretation of dune database records across the subcontinent, Quaternary Int., 410, 30–45, https://doi.org/10.1016/j.quaint.2015.10.011, 2016.

Tierney, J. E., Lewis, S. C., Cook, B. I., LeGrande, A. N. and Schmidt, G. A.: Model, proxy, and isotopic perspectives on the East African Humid Period, Earth Planet. Sci. Lett., 307, 103–112, https://doi.org/10.1016/j.epsl.2011.04.038, 2011.

Tinker, J., De Wit, M. J. and Brown, R.: Mesozoic exhumation of the southern Cape, South Africa, quantified using apatite fission track thermochronology, Tectonophysics, 455, 77–93, https://doi.org/10.1016/j.tecto.2008.04.007, 2008.

Tyson, P. D. and Preston-Whyte, R. A.: The weather and climate of Southern Africa, Oxford University Press, Cape Town, South Africa, 396 pp., 978-0195718065, 2000.

Upadhyay, D., Lucarelli, J., Arnold, A., Flores, R., Bricker, H., Ulrich, R. N., Jesmok, G., Santi, L., Defliese, W., Eagle, R. A., Carroll, H. M., Bateman, J. B., Petryshyn, V., Loyd, S. J., Tang, J., Priyadarshi, A., Elliot, B., Tripati.: Carbonate clumped isotope analysis (Δ_{47}) of 21 carbonate standards determined via gas-source isotope-ratio mass spectrometry on four instrumental configurations using carbonate-based standardization and multiyear data sets, Rapid Commun. Mass Spectrom., 35, 17, e9143. doi:10.1002/rcm.9143, 2021

Urey, H. C.: The thermodynamic properties of isotopic substances, J. Chem. Soc., 562–581, https://doi.org/10.1039/JR9470000562, 1947.

Wiese, R., Hartmann, K., Gummersbach, V. S., Shemang, E. M., Struck, U. and Riedel, F.: Lake highstands in the northern Kalahari, Botswana, during MIS 3b and LGM, Quat. Int., 558, 10–18, https://doi.org/10.1016/j.quaint.2020.08.016, 2020.

Zachos, J. C., Dickens, G. R. and Zeebe, R. E.: An early Cenozoic perspective on greenhouse warming and carbon-cycle dynamics, Nature, 451, 279–283, https://doi.org/10.1038/nature06588, 2008.